

A nonparametrically corrected likelihood for Bayesian spectral analysis of multivariate time series

Yixuan Liu^a, Claudia Kirch^b, Jeong Eun Lee^a, Renate Meyer^a

^a*Department of Statistics, The University of Auckland, 38 Princes Street, Auckland, 1010, New Zealand*

^b*Institute of Mathematical Stochastics, Otto-von-Guericke University Magdeburg, Universitätsplatz 2, Magdeburg, 39106, Germany*

Abstract

This paper presents a novel approach to Bayesian nonparametric spectral analysis of stationary multivariate time series. Starting with a parametric vector-autoregressive model, the parametric likelihood is nonparametrically adjusted in the frequency domain to account for potential deviations from parametric assumptions. We show mutual contiguity of the nonparametrically corrected likelihood, the multivariate Whittle likelihood approximation and the exact likelihood for Gaussian time series. A multivariate extension of the nonparametric Bernstein-Dirichlet process prior for univariate spectral densities to the space of Hermitian positive definite spectral density matrices is specified directly on the correction matrices. An infinite series representation of this prior is then used to develop a Markov chain Monte Carlo algorithm to sample from the posterior distribution. The code is made publicly available for ease of use and reproducibility. With this novel approach we provide a generalization of the multivariate Whittle-likelihood-based method of [Meier et al. \(2020\)](#) as well as an extension of the nonparametrically corrected likelihood for univariate stationary time series of [Kirch et al. \(2019\)](#) to the multivariate case. We demonstrate that the nonparametrically corrected likelihood combines the efficiencies of a parametric with the robustness of a nonparametric model. Its numerical accuracy is illustrated in a comprehensive simulation study. We illustrate its practical advantages by a spectral analysis of two environmental time series data sets: a bivariate time series of the Southern Oscillation Index and fish recruitment and time series of windspeed data at six locations in California.

Keywords: multivariate time series, spectral analysis, Whittle likelihood,

1. Introduction

Statistical models can be classified into *parametric* and *nonparametric* models. Parametric techniques assume a pre-specified model with a finite number of parameters from a particular family of distributions for the data. When the specification is correct, those techniques are powerful and efficient. However, the results of parametric approaches are easily affected by misspecification and their advantages significantly diminished in this case. In contrast, nonparametric techniques do not need to make stringent parametric assumptions about the data generating process. As a result, nonparametric models which can have an infinite number of parameters are better at adapting to varying complexities of the data than parametric approaches.

Parametric approaches – in particular vector autoregressive (VAR) models (Chapter 11 in [Brockwell and Davis \(1991\)](#); Part I in [Lütkepohl \(2005\)](#)) – have been broadly applied in both frequentist ([Meyer and Kreiss \(2015\)](#); [Krampe et al. \(2019\)](#)) and Bayesian ([Koop and Korobilis \(2010\)](#); [Kastner and Huber \(2020\)](#)) inference of multivariate time series. Many nonparametric frequentist approaches have been developed for multivariate time series analysis, especially in the frequency domain ([Berkowitz and Diebold \(1998\)](#); [Jentsch and Kreiss \(2010\)](#); [Fiecas \(2014\)](#); [Jentsch and Politis \(2015\)](#)), by extending various univariate bootstrap and resampling approaches. For instance [Franke and Hardle \(1992\)](#), [Kreiss and Paparoditis \(2003\)](#), [Kirch and Politis \(2011\)](#) [McMurry and Politis \(2010\)](#) and [Dai and Guo \(2004\)](#) generate bootstrap samples with a spectral estimate obtained by smoothing its Cholesky decomposition.

Bayesian nonparametric time series analysis has drawn more attention over the last couple of decades. Many techniques applied in the time domain are based on Hidden Markov models ([Fox et al. \(2011\)](#); [Fox et al. \(2014\)](#); [Aicher et al. \(2019\)](#)) and factor models ([Carvalho et al. \(2008\)](#); [Rodríguez and Dunson \(2011\)](#); [Barigozzi and Hallin \(2016\)](#); [Kalli and Griffin \(2018\)](#)). In the frequency domain, numerous methods have been developed that use the Whittle likelihood ([Whittle \(1957\)](#)) for univariate stationary Gaussian time series such as [Choudhuri et al. \(2004a\)](#), [Rousseau et al. \(2012\)](#), [Cadonna et al. \(2017\)](#), [Kirch et al. \(2019\)](#), [Edwards et al. \(2019\)](#), [Rao and Yang \(2021\)](#) and [Maturana-Russel and Meyer \(2021\)](#). The Whittle likelihood approximates

the Gaussian likelihood by a pseudo-likelihood, making use of the asymptotically independent discrete Fourier coefficients that have variances equal to the spectral density at the corresponding Fourier frequencies. The merits of using the Whittle likelihood are its direct dependence on the spectral density and reduced computational costs compared to the true Gaussian likelihood. The Whittle likelihood has also been extensively applied for the analysis of multivariate stationary time series by diverse approaches such as [Rosen and Stoffer \(2007\)](#), [Krafty and Collinge \(2013\)](#), [Cadonna et al. \(2019\)](#), [Meier et al. \(2020\)](#) and [Hu and Prado \(2023\)](#).

As per the preceding discussion, parametric approaches are more effective than nonparametric ones when the specified model closely matches the true data generating process. However, the performance of parametric methods will significantly degenerate when misspecifications occur. Therefore, we propose a novel method which combines the advantages of both parametric and nonparametric approaches for multivariate spectral density estimation of stationary Gaussian time series using the Bayesian framework. To elaborate, we specify a parametric model for the observations in the time domain (e.g. a VAR model) and propose a nonparametric correction of the parametric likelihood in the frequency domain. We show mutual contiguity of the multivariate Gaussian, the Whittle and the nonparametrically corrected likelihood. In particular, when the parametric working model is independent and identical (i.i.d.) Gaussian white noise, the nonparametrically corrected likelihood reduces to the multivariate Whittle likelihood. Thus, with this new corrected likelihood, we effectively propose a novel generalisation of the multivariate Whittle likelihood. This idea has been applied in the univariate case by [Kirch et al. \(2019\)](#). Following the approach by [Choudhuri et al. \(2004a\)](#), they specified a Bernstein-Dirichlet process prior on the spectral density. However, no direct extension of the Dirichlet process to the multivariate scenario ([Meier, 2018](#)) is available. Therefore, [Meier et al. \(2020\)](#) proposed a Gamma process prior on the space of Hermitian positive definite (Hpd) matrix-valued functions. This prior has been successfully implemented along with the Whittle likelihood in their work for nonparametric Bayesian spectral inference. Nonetheless, the case study in [Meier et al. \(2020\)](#) showed that spectral density estimates based on the multivariate Whittle likelihood and the Hpd Gamma process are generally too smooth to capture peaks and sharp features of the spectra. To address this shortcoming, we adapt the Hpd Gamma process prior and update it with our proposed generalised multivariate Whittle likelihood. This yields significant improvements. In particular,

when the parametric likelihood specified in the time domain is sufficiently close to the true model, our procedure performs almost as efficiently as the pure parametric procedure. On the other hand, in the case of model misspecification, our approach is almost as robust as the pure nonparametric approach. More importantly, in the partially misspecified case, our approach outperforms both nonparametric and parametric models.

The remainder of this article is organised as follows. Section 2 proposes the nonparametrically corrected likelihood used for Bayesian spectral analysis of stationary multivariate time series and states its asymptotic properties. Section 3 specifies the prior and describes the posterior computation. Section 4 provides the simulation result. Section 5 demonstrates the application of our approach to two real case studies. Section 6 gives the conclusion and an outlook for future work. The supplementary material contains the proofs and additional results of the simulation study.

2. Extension of the Multivariate Whittle Likelihood

In this section, we will introduce a likelihood for multivariate stationary time series which nonparametrically corrects a parametric likelihood. It can be regarded as an extension of the multivariate Whittle likelihood. To this end, we first revisit the multivariate version of the Whittle likelihood, which was initially proposed by [Whittle \(1957\)](#) in the univariate case.

2.1. Review of the Whittle likelihood

Let $\{\underline{Z}_t = (Z_{t1}, \dots, Z_{td})^T, t = 0, 1, \dots\}$ be a Gaussian stationary time series in \mathbb{R}^d with zero mean and autocovariance matrix $\mathbf{\Gamma}(h) := \mathbb{E}(\underline{Z}_{t+h}\underline{Z}_t^T) = [\gamma_{ij}(h)]_{i,j=1}^d \in \mathbb{R}^{d \times d}$ for $h \in \mathbb{Z}$. Under the assumption that all autocovariance functions are absolutely summable, i.e., $\sum_{h=-\infty}^{\infty} |\gamma_{ij}(h)| < \infty$ for all i and j , the spectral density matrix of $\{\underline{Z}_t\}$ is given by the Fourier transform of the autocovariance matrix:

$$\mathbf{f}(\omega) = \begin{pmatrix} f_{11}(\omega) & f_{12}(\omega) & \dots & f_{1d}(\omega) \\ f_{21}(\omega) & f_{22}(\omega) & \dots & f_{2d}(\omega) \\ \vdots & \vdots & \ddots & \vdots \\ f_{d1}(\omega) & f_{d2}(\omega) & \dots & f_{dd}(\omega) \end{pmatrix} = \frac{1}{2\pi} \sum_{h=-\infty}^{\infty} \mathbf{\Gamma}(h) \exp(-ih\omega) \quad (1)$$

for $0 \leq \omega \leq 2\pi$. Thus, $\mathbf{f}(\omega)$ is a Hermitian positive definite (HpD) matrix and there is a one-to-one relationship between the spectral density and the

covariance matrix. The diagonal elements of $\mathbf{f}(\omega)$ are real-valued and equal to the marginal spectral densities of each of the d univariate time series. The off-diagonal elements f_{ij} for $i \neq j$ are complex-valued in general and referred to as the cross-spectra of $\{Z_{ti}, t = 0, 1, \dots\}$ and $\{Z_{tj}, t = 0, 1, \dots\}$. Consider a sample $\underline{z}_1, \dots, \underline{z}_n$ of $\{\underline{Z}_t\}$ of size n and denote by $\underline{\mathbf{z}}_n := (\underline{z}_1^T, \dots, \underline{z}_n^T)^T \in \mathbb{R}^{nd}$ the vector of stacked observations. The discrete Fourier transform of $\underline{\mathbf{z}}_n$

$$\tilde{\underline{\mathbf{z}}}_j := \frac{1}{\sqrt{n}} \sum_{t=1}^n \underline{Z}_t \exp(-it\omega_j), \quad \omega_j = \frac{2\pi j}{n} \text{ and } j = 0, \dots, \left\lfloor \frac{n}{2} \right\rfloor \quad (2)$$

provides the *Fourier coefficients* at the *Fourier frequencies* ω_j . It holds that $\tilde{\underline{\mathbf{z}}}_j = \tilde{\underline{\mathbf{z}}}_{n-j}^*$ for even n and $\tilde{\underline{\mathbf{z}}}_j = \tilde{\underline{\mathbf{z}}}_{n-j+1}^*$ for odd n when $j > \lfloor n/2 \rfloor$, so the first $\lfloor n/2 \rfloor$ Fourier coefficients contain the same information as $\underline{\mathbf{z}}_n$. An important concept related to the Fourier coefficients is the *periodogram matrix* (simply as *periodogram* in the following) defined as $I_{nd}(\omega_j) := \frac{1}{2\pi} \tilde{\underline{\mathbf{z}}}_j \tilde{\underline{\mathbf{z}}}_j^*$. According to the well-known asymptotic properties of the Fourier coefficients ([Brockwell and Davis, 1991](#)), the periodograms at different Fourier frequencies are asymptotically independent, the expectations of the periodograms converge to the corresponding spectral density matrices with increasing sample size, that is

$$\mathbb{E}I_{nd}(\omega_j) \rightarrow \mathbf{f}(\omega_j), \quad \text{as } n \rightarrow \infty \quad (3)$$

and the periodograms have Exponential distributions with means $\mathbf{f}(\omega_j)$. Based on the asymptotic distribution of the Fourier coefficients, the Whittle likelihood P_W^n is defined as

$$p_W^n(\tilde{\underline{\mathbf{z}}}_1, \dots, \tilde{\underline{\mathbf{z}}}_N | \mathbf{f}) = \prod_{j=1}^N \frac{1}{\pi^d |2\pi \mathbf{f}(\omega_j)|} \exp \left(-\frac{1}{2\pi} \tilde{\underline{\mathbf{z}}}_j^* \mathbf{f}(\omega_j)^{-1} \tilde{\underline{\mathbf{z}}}_j \right) \quad (4)$$

for $j = 1, \dots, N = \lfloor n/2 \rfloor - 1$. For the purpose of spectral density estimation, the boundary Fourier frequencies $\omega_0 = 0$ and $\omega_{n/2} = \pi$ (the latter for n even) are not considered in (4) since the corresponding Fourier coefficients are proportional to the sample mean and the alternating sample mean, respectively. Under certain assumptions on the time series, the Whittle likelihood provides an approximation to the true likelihood but is exact only in the case of Gaussian white noise ([Shao and Wu, 2007](#)). In contrast to the true Gaussian likelihood, the Whittle likelihood depends directly on the spectral density

matrix. Furthermore, an evaluation of the Whittle likelihood only requires the inversion of n matrices of dimension $d \times d$ instead of the inversion of a $nd \times nd$ matrix for the true Gaussian likelihood. This requires $O(nd^3)$ floating point operations, a significant reduction in computational costs compared to the evaluation of the true Gaussian likelihood.

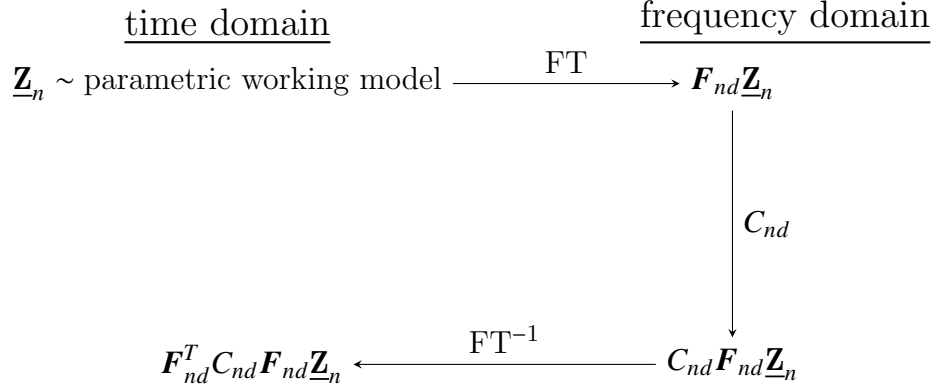
2.2. Nonparametric likelihood correction

For *univariate* time series, a nonparametrically corrected likelihood has already been proposed by Kirch et al. (2019). The idea is to begin with a parametric working likelihood in the time domain and then apply a nonparametric correction in the frequency domain. This is to ensure that the likelihood has the correct second-order dependence structure even if the parametric model is misspecified. Here we propose a nonparametrically corrected likelihood for *multivariate* time series.

To illustrate that the idea stems from the multivariate Whittle likelihood and thus provides an extension and refinement thereof, we first consider multivariate Gaussian white noise, i.e. $\underline{Z}_t \stackrel{iid}{\sim} N_d(\mathbf{0}, \mathbf{I}_d)$, as the parametric working model. Note that the spectral density matrix of this parametric working model is $\frac{1}{2\pi} \mathbf{I}_d$. However, if the model is misspecified, i.e., in the case of coloured noise, the estimate of the spectral density matrix based on this model may not be efficient. Therefore, we nonparametrically correct for potential model misspecification in the frequency domain by multiplying the Fourier coefficients by the square root of a correction matrix and back-transform to the time domain via a discrete inverse Fourier transform. In the case of a white noise working model, the *correction matrix* is defined by the block diagonal matrix

$$C_{nd,W} := (2\pi)^{-1/2} \begin{pmatrix} \mathbf{f}^{1/2}(\omega_1) & & \\ & \ddots & \\ & & \mathbf{f}^{1/2}(\omega_n) \end{pmatrix}.$$

This is illustrated in the diagram below where \mathbf{F}_{nd} denotes the *Fourier transform operator* such that $\mathbf{F}_{nd} \underline{\mathbf{Z}}_n = \tilde{\underline{\mathbf{Z}}}_n$:



As is readily verified, the density induced by the above linear transformation with $C_{nd} = C_{nd,W}$ under the Gaussian white noise working model turns out to be the Whittle likelihood defined in (4), up to the boundary frequencies.

This derivation of the Whittle likelihood as a nonparametrically corrected parametric likelihood provides a way towards a generalization by starting with a more adequate parametric working model than Gaussian white noise. We suggest using a VAR model since the dependence structure of any causal Gaussian linear process can be captured by a VAR model of sufficiently large order. However, any other parametric time series model could be used. Denote by \mathbf{f}_{pa} the spectral density matrix corresponding to the parametric model.

Then the general correction matrix C_{nd} is defined as

$$C_{nd} := \begin{pmatrix} \mathbf{f}^{1/2}(\omega_1) \mathbf{f}_{\text{pa}}^{-1/2}(\omega_1) & & & \\ & \mathbf{f}^{1/2}(\omega_2) \mathbf{f}_{\text{pa}}^{-1/2}(\omega_2) & & \\ & & \ddots & \\ & & & \mathbf{f}^{1/2}(\omega_n) \mathbf{f}_{\text{pa}}^{-1/2}(\omega_n) \end{pmatrix}. \quad (5)$$

Denoting the parametric likelihood of $\underline{\mathbf{Z}}_n$ by p_{pa}^n , the corrected likelihood is given by

$$p_C^n(\underline{\mathbf{Z}}_n | \mathbf{f}, \underline{\mathbf{B}}) \propto |C_{nd} C_{nd}^*|^{-1/2} p_{\text{pa}}^n(\mathbf{F}_{nd}^* C_{nd}^{-1} \mathbf{F}_{nd} \underline{\mathbf{Z}}_n | \underline{\mathbf{B}}), \quad (6)$$

with $\underline{\mathbf{B}}$ being the parameters for the parametric working model.

The following theorem states the properties of the corrected likelihood. Most importantly, the corrected likelihood is equivalent to the parametric

likelihood if the parametric model is the true data-generating model and the periodograms under the corrected likelihood are asymptotically unbiased for the true spectral density matrix regardless of whether the parametric model is correctly specified or not.

Theorem 1. *Let $\underline{\mathbf{Z}}_n \in \mathbb{R}^{nd}$ be a stationary time series with zero mean and spectral density \mathbf{f} . Let $\mathbf{\Gamma}_{nd,pa}$ and \mathbf{f}_{pa} be the autocovariance matrix and the spectral density matrix of a parametric model used in the correction likelihood.*

- (a) *If $\mathbf{f} = \mathbf{f}_{pa}$, then $p_C^n = p_{pa}^n$.*
- (b) *Under the corrected likelihood, the periodogram is an asymptotically unbiased estimator for the true spectral density matrix, i.e.*

$$\mathbb{E}_{p_C^n} I_{nd,\omega_j}(\underline{\mathbf{Z}}_n) = \mathbf{f}(\omega_j) + o(1)$$

holds for $j = 0, \dots, N$.

- (c) *The covariance matrix of the periodogram ordinates under the corrected likelihood is related to the covariance matrix under the parametric likelihood by*

$$\begin{aligned} & \text{Cov}_{p_C^n} \left(I_{nd,\omega_j}(\underline{\mathbf{Z}}_n), I_{nd,\omega_k}(\underline{\mathbf{Z}}_n) \right) \\ &= \text{Cov} \left(\mathbf{C}_{nd,j} I_{nd,\omega_j}(\underline{\mathbf{Y}}_n) \mathbf{C}_{nd,j}^*, \mathbf{C}_{nd,k} I_{nd,\omega_k}(\underline{\mathbf{Y}}_n) \mathbf{C}_{nd,k}^* \right) \end{aligned}$$

for $j, k = 0, \dots, N$, where $\mathbf{C}_{nd,j}$ is the j -th diagonal block of \mathbf{C}_{nd} .

Please refer to the supplementary material for the proof of Theorem 1.

2.3. Mutual contiguity

In this section, we will derive an asymptotic property of the corrected likelihood for *Gaussian* time series, which is useful e.g. for the purpose of studying posterior consistency as in Kirch et al. (2019) and Meier et al. (2020). More precisely, we will prove mutual contiguity of the corrected likelihood, the Whittle likelihood and the full Gaussian likelihood. This is important since mutual contiguity of two probability measures defined on measurable spaces that change with the sample size n implies that those measures have the same asymptotic properties. The main usefulness of showing mutual

contiguity of the corrected likelihood, the Whittle and the true Gaussian likelihood is that if one can prove consistency or find the rate of convergence of an estimator under the Whittle measure, then the estimator is also consistent and has the same rate of convergences under the true Gaussian measure. In the univariate case, mutual contiguity between the true Gaussian likelihood and the Whittle likelihood was proved by [Choudhuri et al. \(2004b\)](#), in which Le Cam's first lemma (see Lemma 6.4 in [van der Vaart \(1998\)](#)) was used. [Meier et al. \(2020\)](#) extended the univariate contiguity to the multivariate case, so it remains to establish mutual contiguity between the corrected likelihood and the Whittle likelihood. To this end, we first state the definition of mutual contiguity and specify the following two assumptions, which are the generalisation of Assumption A.1 in [Kirch et al. \(2019\)](#) to the multivariate case.

Two probability measures P_n and Q_n on measurable spaces Ω_n are *mutually contiguous* if for every sequence of measurable sets A_n , $P_n(A_n) \rightarrow 0$ implies $Q_n(A_n) \rightarrow 0$ and versa vice (cf. Definition 6.3 in [van der Vaart \(1998\)](#)).

Assumption 1. *For the parametric working model, the eigenvalues of the spectral density matrix $\mathbf{f}_{pa}(\cdot)$ are uniformly bounded and uniformly bounded away from 0. That is, there exist positive constants $b_{0,pa}$ and $b_{1,pa}$ such that*

$$\lambda_{\min}(\mathbf{f}_{pa}(\omega)) \geq b_{0,pa}, \quad \lambda_{\max}(\mathbf{f}_{pa}(\omega)) \leq b_{1,pa}, \quad 0 \leq \omega \leq \pi.$$

Moreover, the autocovariance function matrix $\mathbf{\Gamma}_{pa}(\cdot)$ fulfills

$$\sum_{h \in \mathbb{Z}} \|\mathbf{\Gamma}_{pa}(h)\| |h|^a < \infty,$$

for some $a > 1$.

Assumption 2. *The eigenvalues of the underlying true spectral density matrix $\mathbf{f}(\cdot)$ are uniformly bounded and uniformly bounded away from 0. That is, there exist positive constants b_0 and b_1 such that*

$$\lambda_{\min}(\mathbf{f}(\omega)) \geq b_0, \quad \lambda_{\max}(\mathbf{f}(\omega)) \leq b_1, \quad 0 \leq \omega \leq \pi.$$

Moreover, the true autocovariance function matrix $\mathbf{\Gamma}(\cdot)$ fulfills

$$\sum_{h \in \mathbb{Z}} \|\mathbf{\Gamma}(h)\| |h|^a < \infty,$$

for some $a > 1$.

Assumption 2 was used by Meier et al. (2020) to establish the mutual contiguity between the exact Gaussian likelihood and the Whittle likelihood. The restriction on the Frobenius norm of $\mathbf{\Gamma}(\cdot)$ ensures the continuous differentiability of \mathbf{f} with derivative being Hölder of order $a - 1 > 0$. Assumption 1 makes the same restrictions on the parametric working model. Under these two assumptions, we can establish the mutual contiguity.

Theorem 2. *Let $\underline{\mathbf{Z}}_n \in \mathbb{R}^{nd}$ be a time series with zero mean, spectral density matrix \mathbf{f} and autocovariance matrix $\mathbf{\Gamma}_{nd}$ fulfilling Assumption 2. Let \mathbf{f}_{pa} and $\mathbf{\Gamma}_{nd,pa}$ be the spectral density matrix and autocovariance matrix of a Gaussian parametric model fulfilling Assumption 1. Then the true joint density P^n , the joint density P_W^n under the Whittle likelihood and the joint density P_C^n under the corrected likelihood equipped with the Gaussian parametric working model of $\underline{\mathbf{Z}}_n$ are mutually contiguous.*

The proof of Theorem 2 is contained in Section 2 in the supplementary material.

3. Bayesian spectral inference

3.1. Prior specification

For a nonparametric Bayesian approach to spectral density estimation, a nonparametric prior on the space of Hpd matrix-valued functions is required. To this end, we employ the Bernstein-Hpd-Gamma prior introduced by Meier et al. (2020), which combines the Bernstein polynomial and the Hpd-Gamma process. Let $\bar{\mathbf{S}}_d^+$ be the set of $d \times d$ Hermitian positive semidefinite (Hpsd) matrices with unit trace and $\bar{\mathbf{S}}_d^+ \cong \bar{\mathbf{S}}_d^+ \times (0, \infty)$. Let $r \in (0, \infty)$ be the radial part and $\mathbf{U} \in \bar{\mathbf{S}}_d^+$ be the spherical part such that any $\mathbf{Z} \in \bar{\mathbf{S}}_d^+$ can be decomposed as $\mathbf{Z} = r\mathbf{U}$. The Hpd-Gamma distribution $\mathbf{X} \sim \text{Ga}_{d \times d}(\alpha, \beta)$ is defined via its Laplace transform as

$$\mathbb{E} \text{etr}(\mathbf{X}\boldsymbol{\Theta}) = \exp \left\{ - \int_{\bar{\mathbf{S}}_d^+} \int_0^\infty (1 - \text{etr}(-r\boldsymbol{\Theta}\mathbf{U})) \frac{\exp(-\beta(\mathbf{U})r)}{r} dr \alpha(d\mathbf{U}) \right\}$$

for all $\boldsymbol{\Theta} \in \bar{\mathbf{S}}_d^+$ with α on $\bar{\mathbf{S}}_d^+$ and $\beta : \bar{\mathbf{S}}_d^+ \rightarrow (0, \infty)$, where $\text{etr}(\mathbf{X}) := \exp(\text{tr}(\mathbf{X}))$. When $d = 1$, the Hpd-Gamma distribution is the same as the univariate Gamma distribution, so α and β can be regarded as an extension of the scale and rate parameters. Then a random process $\boldsymbol{\Phi} \sim \text{GP}_{d \times d}(\alpha, \beta)$ is called a

Hpd-Gamma process on $\mathcal{X} = [0, \pi]$ if any arbitrary numbers of non-empty partitions of \mathcal{X} are jointly Hpd-Gamma distributed. However, instead of specifying the prior on \mathbf{f} directly, we specify the prior on the Hpd correction matrix defined as

$$\mathbf{Q}(\omega) := \mathbf{f}_{\text{pa}}^{-1/2}(\omega) \mathbf{f}(\omega) \mathbf{f}_{\text{pa}}^{-1/2}(\omega). \quad (7)$$

For $k \in \mathbb{N}$, we equidistantly partition $[0, \pi]$ into k equidistant intervals as

$$I_{j,k} = ((j-1)\pi/k, j\pi/k], \quad j = 1, \dots, k. \quad (8)$$

The *Bernstein-Hpd-Gamma* prior for $\mathbf{Q}(\cdot)$ is defined by

$$\mathbf{Q}(\pi x) := \sum_{j=1}^k \Phi(I_{j,k}) b(x|j, k-j+1), \quad 0 \leq x \leq 1, \quad \text{and} \quad k \sim p(k), \quad (9)$$

where $b(\cdot|j, k-j+1)$ denotes the probability density function of a $\text{Beta}(j, k-j+1)$ distribution. The parameter k is a smoothness parameter, the smaller k , the smoother the resulting matrix-valued function \mathbf{Q} . By putting a discrete prior probability function $p(k)$ on the polynomial degree k , we achieve a data-driven choice of the degree of smoothness.

In the univariate case, a mixture of Bernstein polynomials with weights defined by a Dirichlet process was used by [Choudhuri et al. \(2004a\)](#) and [Kirch et al. \(2019\)](#). Such a Dirichlet process is a normalized Gamma process (see Section 1.2 in [Meier \(2018\)](#)), so the Bernstein-Hpd-Gamma prior can be regarded as a multivariate extension of the Bernstein-Dirichlet process prior on the space of univariate spectral densities to that of spectral density matrices. Analogous to the famous stick-breaking representation of the Dirichlet process, Theorem 4.4 in [Meier et al. \(2020\)](#) shows that under weak assumptions Φ can be represented by an almost surely convergent series involving i.i.d. components as

$$\begin{aligned} \Phi &\stackrel{\text{a.s.}}{=} \sum_{j=1}^{\infty} \delta_{x_j} r_j \mathbf{U}_j, \quad (x_j, \mathbf{U}_j) \stackrel{i.i.d.}{\sim} \alpha^* \\ r_j &= \rho^-(w_j | C_\alpha, \beta(x_j, \mathbf{U}_j)), \quad w_j = \sum_{i=1}^j v_i, \quad v_i \stackrel{i.i.d.}{\sim} \text{Exp}(1), \end{aligned} \quad (10)$$

where

$$\alpha^* := \alpha/C_\alpha, \quad C_\alpha := \int_{\mathcal{X}} \alpha(x, \bar{\mathbf{S}}_d^+) dx,$$

$$\rho^-(w|a, b) = \inf\{r > 0 : \rho([r, \infty]|a, b) < w\}, \quad \rho(dr|a, b) = a \frac{\exp(-br)}{r} dr.$$

A truncation of the infinite series allows the design of a MCMC algorithm to sample from the posterior distribution as described in Section 3.2.

By putting a prior on the parameters of the parametric working model, both parametric and nonparametric components of the model can be inferred simultaneously. This has been considered in the univariate corrected likelihood procedure by Kirch et al. (2019), in which the working model is an autoregressive (AR) time series model and the prior is put on the partial autocorrelations to ensure stationarity and causality. Similarly, in the multivariate case, we can use the VAR time series model as our parametric working model. This parametric model has also been used for the multiple hybrid bootstrap by Jentsch and Kreiss (2010). To elaborate, recall that the equation of a VAR(p) model with $p \geq 1$ and Gaussian innovation is defined as

$$\underline{Z}_t = \sum_{j=1}^p \mathbf{B}_j \underline{Z}_{t-j} + \underline{\varepsilon}_t, \quad \underline{\varepsilon}_t \stackrel{i.i.d.}{\sim} N_d(\underline{0}, \underline{\Sigma}), \quad t = p+1, \dots, n \quad (11)$$

with innovation covariance $\underline{\Sigma} \in \mathcal{S}_d^+(\mathbb{R})$ and the coefficient matrices

$$\mathbf{B}_j = \begin{pmatrix} B_{j,1,1} & \cdots & B_{j,1,d} \\ \vdots & \ddots & \vdots \\ B_{j,d,1} & \cdots & B_{j,d,d} \end{pmatrix}$$

$\mathbf{B}_1, \dots, \mathbf{B}_p \in \mathbb{R}^{d \times d}$ with $\mathbf{B}_p \neq \mathbf{0}$. Consider a vector

$$\underline{\beta} = (B_{1,1,1}, \dots, B_{1,1,d}, B_{2,1,1}, \dots, B_{2,1,d}, \dots, B_{p,1,d}, B_{1,2,1}, \dots, B_{p,d,d})^T \in \mathbb{R}^{pd^2},$$

which stacks all the VAR coefficients of (11). In the implementation, the VAR order p is predetermined by some order selection criteria, such as Akaike's Information Criterion (AIC) by Akaike (1974) or the elbow criterion (see Section 6). For the coefficients, we assume

$$\underline{\beta} \sim N(\underline{\mu}_\beta, \mathbf{V}_\beta), \quad (12)$$

so that the prior is parametrised by $\boldsymbol{\beta}$ and \mathbf{V}_β . We use a noninformative prior by setting $\boldsymbol{\mu}_\beta = \mathbf{0} \in \mathbb{R}^{pd^2}$ and $\mathbf{V}_\beta^{-1} \approx \mathbf{0} \in \mathbb{R}^{pd^2 \times pd^2}$.

3.2. Posterior computation

To implement an MCMC algorithm, we truncate the representation of Φ in (10) at some large L such that $\Phi \approx \sum_{l=1}^L \delta_{x_l} r_l \mathbf{U}_l$. The value of L should be determined by considering the sample size and the error tolerance in practical computations. A conservative truncation choice is $L = \max\{20, n^{1/3}\}$. In fact, that choice is used in the stick-breaking representation of the Dirichlet process found by [Muliere and Tardella \(1998\)](#) and [Choudhuri et al. \(2004a\)](#). As a result, the posterior distribution combined with the prior of k and the corrected likelihood (6) follows

$$p_C(\underline{\Theta}_\Phi, k | \underline{\mathbf{Z}}_n, \underline{\mathbf{B}}) \propto p_C^n(\underline{\mathbf{Z}}_n | \underline{\Theta}_\Phi, k, \underline{\mathbf{B}}) p(\underline{\Theta}_\Phi) p(k) p(\underline{\mathbf{B}}) \quad (13)$$

with $\underline{\Theta}_\Phi := (x_1, \dots, x_L, r_1, \dots, r_L, \mathbf{U}_1, \dots, \mathbf{U}_L)$ being the parameter space of Φ is composed of $3L$ parameters and $\underline{\mathbf{B}} = (\mathbf{B}_1, \dots, \mathbf{B}_p)$ containing the parameters of the VAR parametric working model with order $p \geq 1$.

Remark 1. *In the univariate case, for reasons of identifiability, it is important to use a parametric working model with standardised errors, i.e., with $\sigma = 1$, because all choices for σ lead to the same corrected likelihood. This eliminates the need of pre-estimating or putting a prior on the error variance. However, the situation is more involved in the multivariate case as two different covariance matrices can lead to different corrected likelihoods. This is because two covariance matrices can differ by more than just a multiplicative constant and, indeed, two correlation matrices can have a very different structure. Based on some pilot simulation studies, putting a prior on the innovation term results in a high computational demand and can cause difficulty in posterior convergence (possibly due to some additional non-identifiability beyond multiplicative constants). Therefore, we pre-estimate the covariance of the innovation term and do not update it in the MCMC algorithm. The simulation results and the case studies in Sections 5 and 6 show that this implementation with a fixed (pre-estimated) innovation covariance performs well.*

3.3. A Metropolis-within-Gibbs algorithm

We use Metropolis-Hastings (MH) steps (Hastings (1970)) to update the full conditionals in the Gibbs sampler, a Metropolis-within-Gibbs algorithm (Tierney (1994)). To elaborate, we will use the same algorithm to infer Φ and k as Meier et al. (2020), in which U_j 's are reparametrised by some hyperspherical coordinates φ_j 's. The multivariate normal random walk is used for the full conditional for the coefficients of the parametric working model. Algorithm 1 summarises the algorithm of sampling from the posterior. For more details, please see <https://github.com/easycure1/vnpctest>.

Algorithm 1 MCMC algorithm

Initialise $k^{(1)}, (r_1^{(1)}, \dots, r_L^{(1)}), (x_1^{(1)}, \dots, x_L^{(1)}), (\varphi_1^{(1)}, \dots, \varphi_L^{(1)})$ and $(\mathbf{B}_1^{(1)}, \dots, \mathbf{B}_p^{(1)})$.
Start Gibbs sampling
while $i \leq N$ **do**
 Propose $k^{*,(i+1)}$ using random walk restricted by a sufficiently upper limit k_{\max} .
 Update $k^{(i+1)}$ in the MH-step by calculating (13).
 while $l \leq L$ **do**
 Propose $r_l^{*,(i+1)}$ using the log-normal random walk with the scale parameter updated during the burn-in period.
 Update $r_l^{(i+1)}$ in the MH-step by calculating (13).
 end while
 while $l \leq L$ **do**
 Propose $x_l^{*,(i+1)}$ using the uniform random walk with scale parameter $\delta_{x_l} := \frac{\pi l}{l+2\sqrt{n}}$.
 Update $x_l^{(i+1)}$ in the MH-step by calculating (13).
 end while
 while $l \leq L$ **do**
 Propose $\varphi_l^{*,(i+1)}$ using the uniform random walk with the scale parameter updated during the burn-in period.
 Update $\varphi_l^{(i+1)}$ in the MH-step by calculating (13).
 end while
 while $j \leq p$ **do**
 Propose $\mathbf{B}_j^{*,(i+1)}$ using the multivariate normal random walk with the scale parameter updated during the burn-in period.
 Update $\mathbf{B}_j^{(i+1)}$ in the MH-step by calculating (13).
 end while
end while

4. Simulation study

In the simulation study, we compare the corrected likelihood approach to the parametric VAR approach and the nonparametric Whittle likelihood approach proposed by Meier et al. (2020) in the case of a correctly specified parametric model and a misspecified one. To this end, we first introduce some criteria used for quantifying the estimation performance, and

the corresponding results for the posterior will be summarised in Section 4.3. The implementation of this approach is available at <https://github.com/easycure1/vnpctest> while the other two approaches are included in the R package `beyondWhittle` on CRAN (Meier et al. (2022)).

Consider a posterior spectral density matrix sample $\mathbf{f}^{(1)}(\omega), \dots, \mathbf{f}^{(M)}(\omega)$ at any given frequency ω . Let \mathcal{S}_d^+ be the set of $d \times d$ Hp_d matrices. Consider the mapping $\mathcal{H} : \mathcal{S}_d \rightarrow \mathbb{R}^{d \times d}$ ¹ such that the real parts above the diagonal of an Hp_d matrix \mathbf{A} will remain above the diagonal of $\mathcal{H}\mathbf{A}$, the imaginary parts above the diagonal of \mathbf{A} will be assigned to below the diagonal of $\mathcal{H}\mathbf{A}$ and the diagonal entries of \mathbf{A} stay in the same position in $\mathcal{H}\mathbf{A}$. Denote the image of the sample $\mathbf{f}^{(j)}(\omega)$ via \mathcal{H} by $\underline{h}^{(j)} := \mathcal{H}\mathbf{f}^{(j)}(\omega)$ for $j = 1, \dots, M$. Assume that $\underline{h}^{(j)}$ has entries $\{h_1^{(j)}, \dots, h_{d^2}^{(j)}\}$. Let $\hat{\underline{h}}$ be the median of all $\underline{h}^{(1)}, \dots, \underline{h}^{(M)}$ so that \hat{h}_k is the median of $\{h_k^{(1)}, \dots, h_k^{(M)}\}$ for $k = 1, \dots, d^2$. Then we call $\hat{\mathbf{f}}_0(\omega) := \mathcal{H}^{-1}\hat{\underline{h}}$ the *pointwise median spectral density matrix* of $\mathbf{f}^{(1)}(\omega), \dots, \mathbf{f}^{(M)}(\omega)$. In the following contents, $\hat{\mathbf{f}}_0$ will be regularly used as a Bayes estimator for the true spectral density matrix \mathbf{f}_0 . To measure the goodness of $\hat{\mathbf{f}}_0$, we consider the corresponding \mathbf{L}_1 - and \mathbf{L}_2 -errors.

We are also interested in the uncertainty of the posterior estimate. To this end, based on the posterior sample, we construct *pointwise 90% credible regions* for the spectral density matrix, where pointwise refers to the frequency. Additionally, we construct *uniform 90% credible regions* as follows: Denote by $\hat{\sigma}_k(\omega)$ the median absolute deviation of $\{h_k^{(1)}(\omega), \dots, h_k^{(M)}(\omega)\}$ for $0 \leq \omega \leq \pi$ and $k = 1, \dots, d^2$. Let $\hat{\sigma} := (\hat{\sigma}_1, \dots, \hat{\sigma}_{d^2})$. We consider the smallest positive number $\xi_{0.9}$ such that

$$\frac{1}{M} \sum_{j=1}^M \mathbb{1} \left\{ \max_{\substack{0 \leq \omega \leq \pi \\ k=1, \dots, d^2}} \frac{|h_k^{(j)}(\omega) - \hat{h}_k(\omega)|}{\hat{\sigma}_k(\omega)} \leq \xi_{0.9} \right\} \geq 0.9.$$

Let $\underline{\hat{h}}^{[0.05]} := \underline{\hat{h}} - \xi_{0.9} \hat{\sigma}$ and $\underline{\hat{h}}^{[0.95]} := \underline{\hat{h}} + \xi_{0.9} \hat{\sigma}$. As well, let $\tilde{\mathbf{f}}_0^{[0.05]} := \mathcal{H}^{-1} \underline{\hat{h}}^{[0.05]}$ and $\tilde{\mathbf{f}}_0^{[0.95]} := \mathcal{H}^{-1} \underline{\hat{h}}^{[0.95]}$. Then, the region between $\tilde{\mathbf{f}}_0^{[0.05]}$ and $\tilde{\mathbf{f}}_0^{[0.95]}$, i.e.

$$\mathcal{C}_{\text{uni}}(\omega|0.9) := \left\{ t \tilde{\mathbf{f}}_0^{[0.05]}(\omega) + (1-t) \tilde{\mathbf{f}}_0^{[0.95]}(\omega) : 0 \leq t \leq 1 \right\}, \quad 0 \leq \omega \leq \pi$$

is the uniform 90% credible region.

¹CK: It might be easier to give the formula instead of a text explanation that goes over 4 lines

4.1. Prior choice

The prior probability of k is chosen as $p(k) \propto \exp(-0.01k \log k)$. For practical feasibility, we employ the $A\Gamma$ -process $A\Gamma(\eta, \omega, \Sigma)$ (see Remark 4.1 in [Meier et al. \(2020\)](#) for details) as the prior for Φ . In particular, the parameters of $A\Gamma(\eta, \omega, \Sigma)$ are chosen as $\eta = d$, $\omega = d$ and $\Sigma = 10^4 \mathbf{I}_d$. Furthermore, to improve the robustness at the boundary, we employ the truncated Bernstein prior

$$\mathcal{Q}_{\tau_l}^{\tau_r}(\pi x) := \sum_{j=1}^k \Phi(I_{j,k}) b_{\tau_l}^{\tau_r}(x|j, k-j+1), \quad 0 \leq x \leq 1, \quad \text{and} \quad k \sim p(k)$$

with $\tau_l = 0.1$ and $\tau_r = 0.9$.

In the implementation, we run 80,000 iterations for the Markov Chain, and the first 30,000 iterations are discarded after the burn-in period. The remaining 50,000 samples are thinned by taking every 5-th value in order to reduce the amount of memory used. We set $k_{\max} = 300$ and $L = 20$.

4.2. Simulated data

The following two bivariate models are used to generate the simulated multivariate time series:

a) VAR2 model

$$\underline{Z}_t = \begin{pmatrix} 0.5 & 0 \\ 0 & -0.3 \end{pmatrix} \underline{Z}_{t-1} + \begin{pmatrix} 0 & 0 \\ 0 & -0.5 \end{pmatrix} \underline{Z}_{t-2} + \underline{e}_t, \quad \underline{e}_t \stackrel{iid}{\sim} N\left(\mathbf{0}, \begin{pmatrix} 1 & 0.9 \\ 0.9 & 1 \end{pmatrix}\right); \quad (14)$$

b) VMA(1) model

$$\underline{Z}_t = \underline{e}_t + \begin{pmatrix} -0.75 & 0.5 \\ 0.5 & 0.75 \end{pmatrix} \underline{e}_{t-1}, \quad \underline{e}_t \stackrel{iid}{\sim} N\left(\mathbf{0}, \begin{pmatrix} 1 & 0.5 \\ 0.5 & 1 \end{pmatrix}\right). \quad (15)$$

These two models have also been considered by [Meier et al. \(2020\)](#) for the comparison between VNP and VAR. The VMA(1) model is a simple linear multivariate time series example, and it does not belong to the family of VAR models, which are used by the VAR procedure and the parametric working model for our VNPC procedure. We use a fixed small order for the parametric working model of the VNPC procedure while the order of the parametric VAR approach is selected by AIC.

We consider three different sample sizes, $n = 256, n = 512$ and $n = 1024$. For each sample size, $N = 500$ independent realisations are generated for both the VAR(2) and VMA(1) models. One realisation of length $n = 256$ of each model (14) and (15) is given in Figure 1.

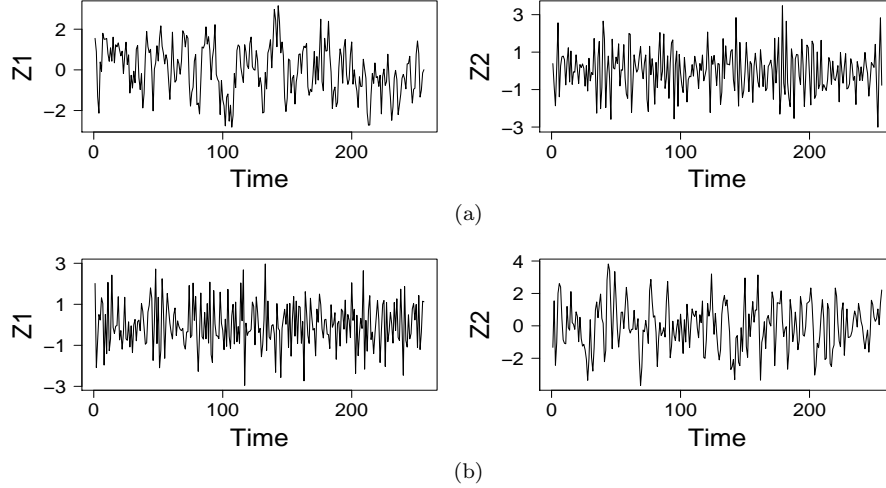


Figure 1: Realisation of (a) the VAR(2) model (14) and (b) the VMA(1) model (15) of length $n = 256$. The left panel displays the first component and the right panel the second component of the time series.

4.3. Results

The results of the simulation study are shown in Table 1. As to be expected, for the correctly specified VAR(2) model, the parametric VAR procedure has much smaller L_1 - and L_2 -errors than the other two nonparametric procedures. The VNP and the VNPC procedures show almost the same performance in this case. For the data generated from a VMA(1) model, a large order p was selected by AIC to fit a VAR(p) model in this misspecified case. The estimates based on the VNPC and the VNP model have smaller L_1 - and L_2 -errors than the VAR model. The VNPC model outperforms the nonparametric VNP estimate as it can benefit from the partially correct VAR(1) working model.

Table 1 also shows the empirical coverage of uniform 90% credible regions and the median (among replications) of the median (over all frequencies) width of uniform 90% credible regions for all procedures. Not surprisingly, for the correctly specified case, the empirical coverage of the VAR credible

intervals attain the nominal level. In the misspecified VMA(1) case, the coverage of the VAR procedure is even larger due to the enlarged width. The VNP procedure produces similar coverages with smaller widths in either of the two cases. As discussed in Szabó et al. (2015), to produce *honest* (in the sense that their coverage matches (approximately) the corresponding posterior probability mass of the regions, 90% in our case) credible sets in the nonparametric setting, the prior has to be selected to slightly undersmooth. However, the Bernstein polynomials used in the mixture prior in the VNP procedure tend to oversmooth the true spectral density, so it might not be appropriate for achieving an honest credible region. As a comparison, the VNPC procedure enhances the coverage sufficiently to almost 90% for both cases.

	VAR(2) model								
	$n = 256$			$n = 512$			$n = 1024$		
	VNPC(1)	VNP	VAR	VNPC(1)	VNP	VAR	VNPC(1)	VNP	VAR
L_1 -error	0.099	0.106	0.075	0.076	0.081	0.051	0.059	0.063	0.036
L_2 -error	0.130	0.136	0.099	0.101	0.106	0.067	0.080	0.084	0.047
Coverage	0.826	0.548	0.908	0.718	0.374	0.898	0.616	0.348	0.886
Width \mathbf{f}_{11}	0.341	0.314	0.210	0.177	0.168	0.121	0.109	0.104	0.078
Width $\Re \mathbf{f}_{12}$	0.258	0.235	0.146	0.171	0.159	0.086	0.119	0.113	0.054
Width $\Im \mathbf{f}_{12}$	0.212	0.187	0.122	0.142	0.128	0.076	0.097	0.090	0.051
Width \mathbf{f}_{22}	0.499	0.445	0.196	0.267	0.257	0.110	0.166	0.166	0.071
	VMA(1) model								
	$n = 256$			$n = 512$			$n = 1024$		
	VNPC(1)	VNP	VAR	VNPC(1)	VNP	VAR	VNPC(1)	VNP	VAR
L_1 -error	0.081	0.097	0.156	0.060	0.072	0.121	0.049	0.055	0.093
L_2 -error	0.102	0.117	0.189	0.076	0.087	0.144	0.062	0.065	0.110
Coverage	0.888	0.594	0.980	0.876	0.518	0.972	0.690	0.294	0.966
Width \mathbf{f}_{11}	0.346	0.299	1.313	0.200	0.194	0.661	0.129	0.135	0.406
Width $\Re \mathbf{f}_{12}$	0.232	0.211	0.609	0.139	0.141	0.414	0.087	0.099	0.287
Width $\Im \mathbf{f}_{12}$	0.172	0.128	0.454	0.101	0.101	0.311	0.066	0.082	0.218
Width \mathbf{f}_{22}	0.498	0.462	1.890	0.299	0.301	1.008	0.193	0.213	0.625

Table 1: Average L_1 -, L_2 -errors, empirical coverages and median width of uniform 90% credible regions of the VNPC estimates with fixed parametric working model order 1, the VNP, and the VAR estimates with order selected by AIC for $N = 500$ realisations of the VAR(2) model (14) and the VMA(1) model (15).

Spectral density estimates obtained by the three procedures for one random realisation of each of the two models are displayed in the supplementary material. Moreover, an additional simulation study in Section 1 in the supplementary material shows that the VNPC procedure using a Gaussian VAR working model performs well even in the misspecified case when the data-generating process is non-Gaussian.

5. Case studies

Here we demonstrate the proposed Bayesian nonparametric approach based on the corrected multivariate likelihood on a bivariate time series that has been extensively studied in the literature and a six-dimensional times series of windspeed measurements. Section 5.1 first introduces a method to choose the order of the parametric VAR(p) working model of the VNPC approach. Both studies use the same prior settings as the simulation study (see Section 4.1).

5.1. Elbow criterion

Under some weak assumptions, the VAR(p) model with sufficiently large order p can capture the dependence structure of a Gaussian linear process to any degree of accuracy. Accordingly, using a VAR model with a sufficiently large order can be regarded as a nonparametric procedure. This result has been employed by the VAR-sieve-bootstrap method proposed by Meyer and Kreiss (2015). In addition, that result also implies that the misspecified VAR model can still be used for the spectral density matrix estimation if the order is chosen to be sufficiently large. This explains why standard model selection techniques such as AIC tend to return a large order when misspecification occurs. This can lead to increased computational time, while also potentially causing the procedure to exhibit excessive confidence in the parametric model. Hence, we want to use a relatively small order for the parametric working model in our corrected likelihood procedure that is capable of describing the main features but not minute detail of the data. With this objective in mind, we follow the order selection approach used by the univariate corrected likelihood procedure in Kirch et al. (2019), which applies a rule-of-thumb rule to check for a bend or elbow in a plot of model order versus negative maximum log-likelihood evaluated at the least squares estimates. To elaborate, in most cases we will see an obvious bend in this scree-like plot as the order increases. The penalty term of standard penalisation techniques is tuned to find the best fit but too small to find the elbow at which only the most obvious features are explained. In analogy to Principal Components Analysis (PCA), which uses the scree plot to reduce the dimension, we can also use the order where we see a clear bend in the negative maximum log-likelihood plot. With the corresponding autoregressive order, the main features of the data are captured and increasing the number

of parameters further will contribute very little to the corrected likelihood procedure except computational costs.

5.2. Southern oscillation index

The Southern Oscillation Index (SOI) and the associated recruitment series are two simultaneously recorded series used to explore the El Niño cycle ([Shumway and Stoffer \(2011\)](#)). The SOI is a standardised index of sea level air pressure differences between Tahiti and Darwin, Australia. The index is related to the El Niño Southern Oscillation (ENSO), the movement of equatorial sea surface temperature across the Pacific Ocean and its atmospheric response. ENSO is known to be periodically occurring every 2-7 years and last 6-18 months, and it contains three phases: neutral, El Niño (the warm phase) and La Niña (the cool phase) ([National Oceanic and Atmospheric Administration \(2022\)](#); [Statistics New Zealand \(2020\)](#)). ENSO is an extremely important meteorological movement in the Pacific Ocean as it has an impact on the weather through changes in air pressure, sea temperature and wind direction. Due to the periodic behaviour of ENSO, the observations in the SOI series are expected to have a time-dependent structure. For our analysis, we make the same simplifying assumption as [Rosen and Stoffer \(2007\)](#) that all effects (e.g. the seasonal effect) can be represented by the autocovariance structure. The recruitment series is composed of the number of newly spawned fish, re-scaled to the interval $[0, 100]$ as shown in Figure 2. It is believed that the fish spawn is associated with the water temperature so we can expect a cross-dependence between the SOI and the recruitment series. Both series consist of a period of 453 monthly values over the years 1950-1987, which are shown in Figure 2. The data is available in the R package `astsa` as datasets `soi` and `rec` ([Stoffer \(2022\)](#)).

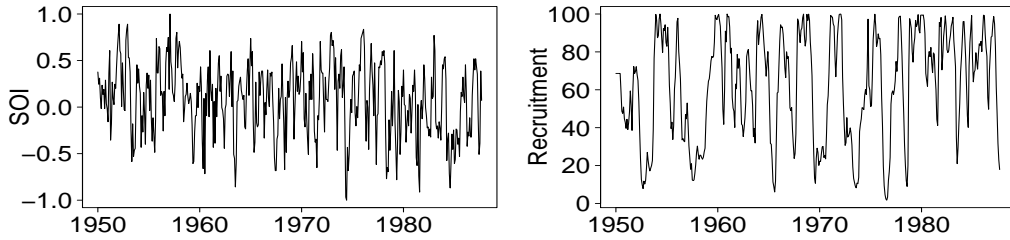


Figure 2: The SOI and recruitment series

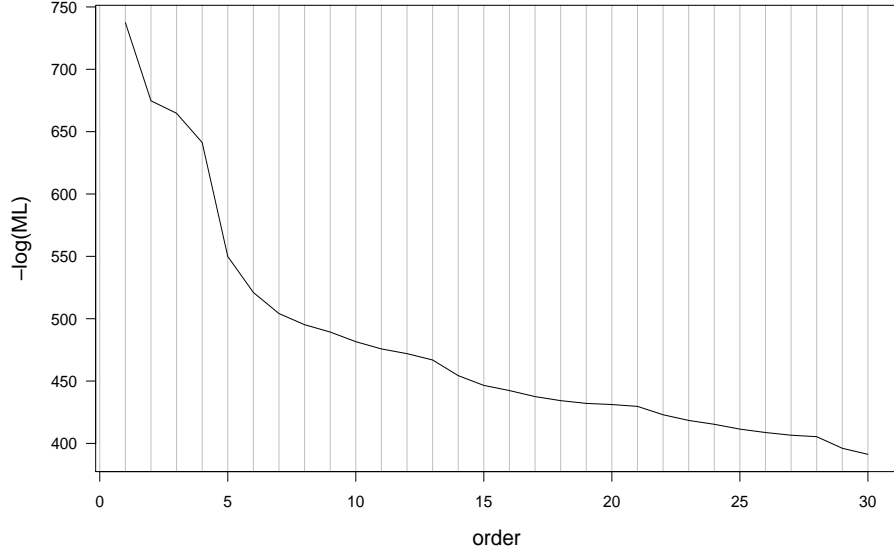


Figure 3: Negative maximum log likelihood for different VAR(p) models applied to the SOI and Recruitment series.

Here, the standardised bivariate time series is analysed. We employ the VNPC procedure with four orders ($p = 0, 2, 5$ and 15) for the parametric working model and the VAR procedure with three orders ($p = 2, 5$ and 15), and we compare the performance of those two procedures. In fact, when the order of the parametric working model is 0, the VNPC procedure is the same as the VNP procedure. The order of 5 is chosen by the elbow criterion (in Figure 3, there is a significant bend at that order). The order of 15 is chosen by minimising the AIC. The arrangement of the bivariate time series is the SOI to be the first series and the recruitment to be the second. To make the comparison for the three procedures with different orders, we demonstrate the results of the two series separately, the SOI in Figure 4 and the recruitment series in Figure 5. It should be noted that since both series are monthly data, the frequency corresponding to a year period within $[0, 2\pi]$ is $\omega_{\text{yearly}} := 2\pi/12 \approx 0.52$.

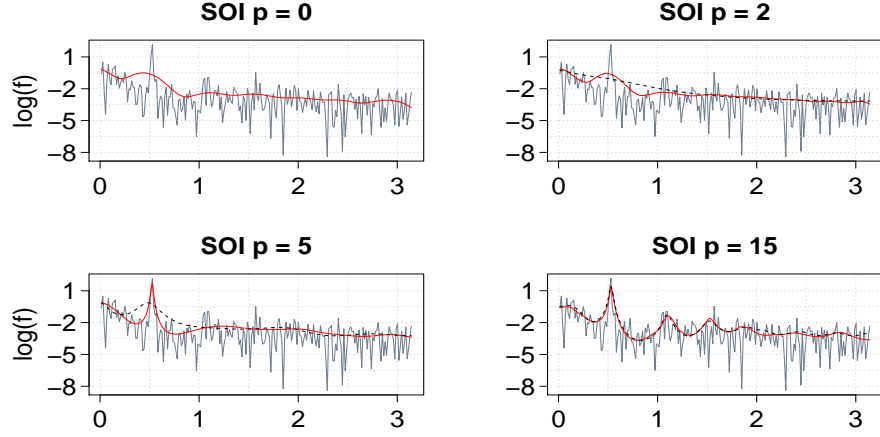


Figure 4: Logarithmic spectral estimates for the SOI series by the VNPC(p) procedure (red line) and the VAR(p) procedure (black dashed line). The periodogram is given in grey.

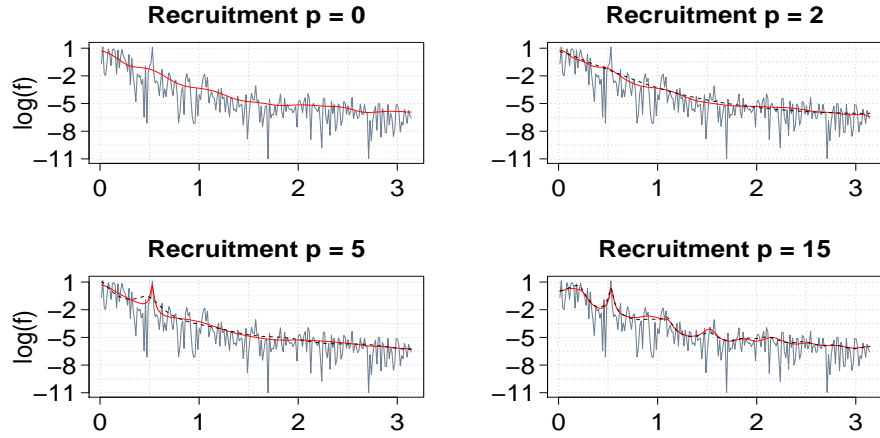


Figure 5: Logarithmic spectral estimates for the recruitment series by the VNPC(p) procedure (red line) and the VAR(p) procedure (black dashed line). The periodogram is given in grey.

From the periodograms of SOI in Figure 4, it can be seen that there is an annual peak. The peak is detected by the VNP procedure, while the spectral

density estimate is overly smooth. However, when $p = 2$, the VAR procedure performs even worse as it is too smooth to pick up any spectral density peaks. In this case, the VNPC procedure with $p = 2$ does not improve much compared to VNP, i.e., VNPC with $p = 0$. When the order is increased to 5, which is the relatively small order chosen by the elbow criterion, the VNPC procedure has successfully estimated the main annual peak, in contrast to the VAR procedure. When using the large order given by AIC, i.e., $p = 15$, the performances of the VNPC and the VAR procedures are very similar. Both estimators pick up the annual peak and its harmonics as well as a broader low-frequency that can be interpreted as the El Niño effect which occurs irregularly every 2–7 years. The findings for the recruitment series in Figure 5 are similar. The VNPC procedure can make use of the relatively small VAR order, $p = 5$, to capture the main annual peak in that series, while the estimates obtained by the VAR procedure with that order are too smooth. Figure 6 provides the 90% pointwise region for VNPC with $p = 5$. The top-right plot displays the real part of the cross-spectrum, which is called the *cospectrum*; and the bottom-left plot displays the imaginary part of the cross-spectrum, which is called the *quadrature spectrum*.

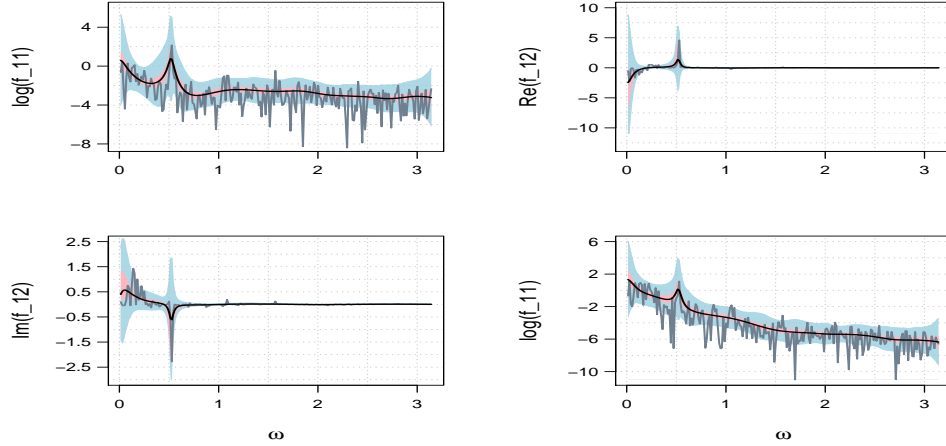


Figure 6: Posterior credible regions for the SOI and recruitment series for the VNPC procedure with a parametric working model with order 5. The diagonal pair shows the logarithmic spectral estimate for the two series and the off-diagonal pair displays the real and imaginary parts of the cross-spectrum. Pointwise 90% regions are visualised in shaded pink and uniform 90% regions are in shaded blue. The posterior median is given by the black solid line and the periodogram is shown in grey.

The *squared coherency* is more adequate for investigating the correlation between two series than the cospectrum and the quadrature spectrum. Recall that the coherency κ between two series at frequency ω is defined as

$$\kappa(\omega|\mathbf{f}) := \frac{f_{12}(\omega)}{(f_{11}(\omega)f_{22}(\omega))^{1/2}}, \quad 0 \leq \omega \leq \pi. \quad (16)$$

This statistic can be viewed as the counterpart of the cross-correlation function in the time domain and it holds $|\kappa(\omega|\mathbf{f})|^2 \leq 1$ for all $0 \leq \omega \leq \pi$ (see Section 11.6 in [Brockwell and Davis \(1991\)](#)). We calculate the squared coherency for all 5000 spectral density estimates and then consider the median and the 90% pointwise region. The result in Figure 7 shows that there is an obvious peak at ω_{yearly} , and this agrees with the findings by the cospectrum and the quadrature spectrum in Figure 7. There are also a few minor peaks at the higher frequencies, which are the harmonics of ω_{yearly} , and the two series are correlated at those frequencies as well. In addition, the strong coherency shown at the low frequencies close to 0 might be because of the 2–7 years El Niño period mentioned previously. In fact, all the results in this Section are in line with the findings in [Rosen and Stoffer \(2007\)](#).

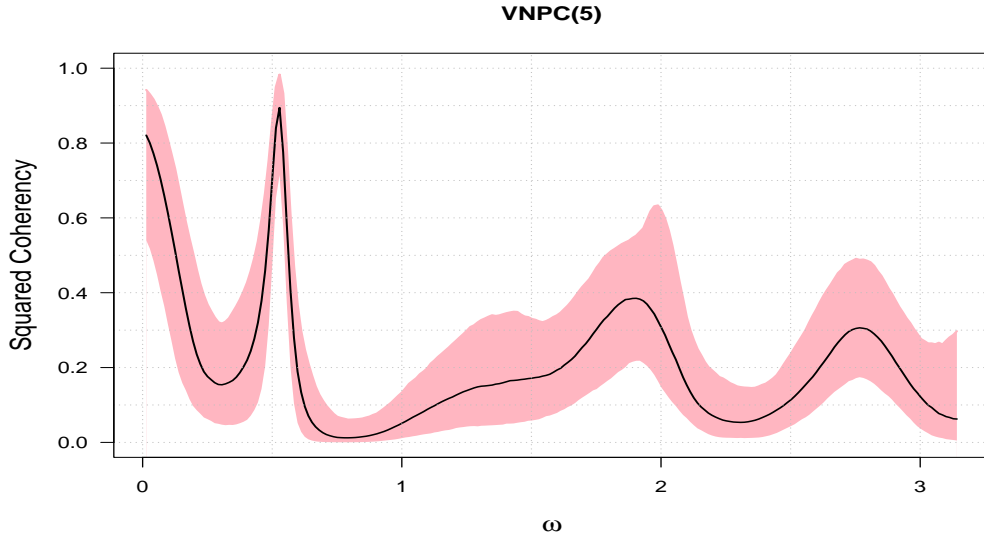


Figure 7: Estimated squared coherency for the SOI and recruitment series by the VNPC procedure with a parametric working model with order 5. The posterior median is given by the black line and the pointwise 90% credible region is in shaded pink.

5.3. Wind speed profiles

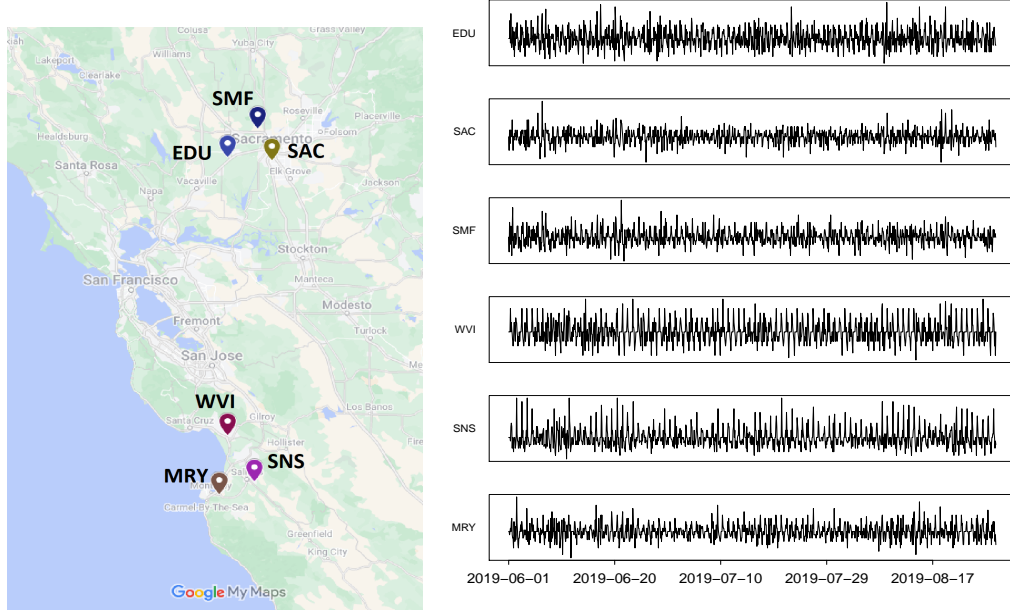


Figure 8: The left graph shows the geographical locations for the six airports. The right graph shows the standardised first differences of median wind speed measurements every two hours from 01-06-2019 12:00 am to 31-08-2019 11:59 pm.

In this case study, we apply the VNPC method to the California wind speed data from the Iowa State University Environmental Mesonet (IEM) Automated Surface System (ASOS) database ([Iowa State University \(2022\)](#); [Mannarano \(1998\)](#)). This example has been studied by [Hu and Prado \(2023\)](#) using a stochastic gradient variational Bayes approach for fast Bayesian inference. In their work, they consider the wind speed in knots at six airports in California from 01-06-2019 12:00 am to 31-08-2019 11:59 pm: EDU (Davis), SAC and SMF (Sacramento), MRY (Monterey), SNS (Salinas), and WVI (Watsonville). That particular time interval is used to avoid extreme values and non-stationarities caused by rainfall and storms, which occurred in other months. In particular, they apply their method to the standardised first difference of median wind speed every two hours for each location. In our study, we use the same processed data, which is accessible from the supplementary material in [Hu and Prado \(2023\)](#). Figure 8 shows the geographical locations for those six airports and the standardised detrended data. All six series are

treated as a six-dimensional time series and analysed simultaneously. The order for the parametric working model suggested by the elbow criterion is 10 (see Figure 9).

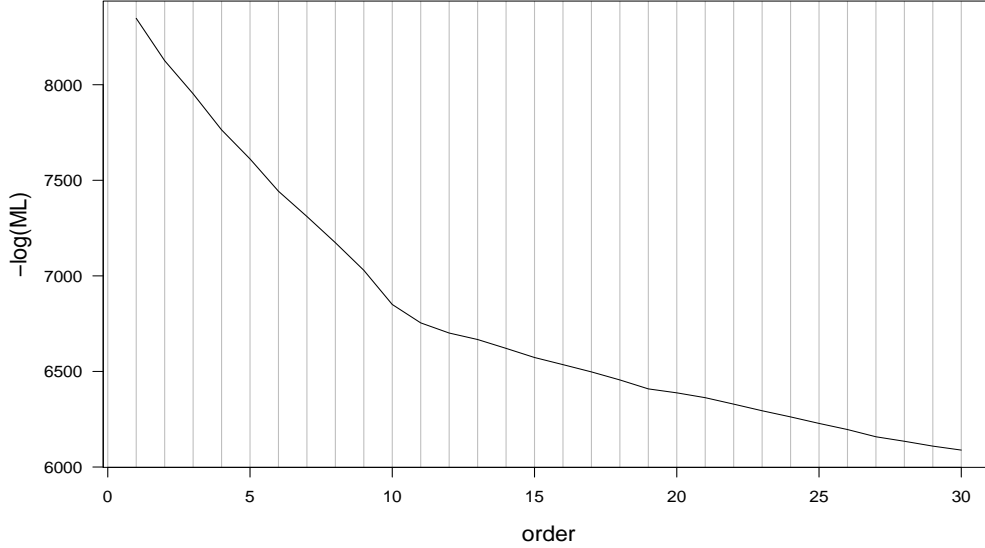


Figure 9: Negative maximum log likelihood for different VAR(p) models applied for the standardised detrended wind speed data.

The results in Figure 10 show that all six spectral densities have a prominent peak at around $2\pi/12 \approx 0.524$, which indicates a strong daily period of wind profile patterns at all locations. This is consistent with the finding in Hu and Prado (2023). However, in contrast to spectral estimates obtained by variational inference in Hu and Prado (2023), peaks in the VPNC estimates are much more pronounced and sharper, for the main daily peak as well as its harmonics. The spectral estimates at $2\pi/12 \approx 0.524$ for the coastal locations WVI, SNS and MRY have slightly larger power than for the inland airports as also noted by Hu and Prado (2023). Furthermore, we are interested in the squared coherencies between the windspeeds at the various pairs of airports. The estimates are given in Figure 11. Not surprisingly, all pairs have a strong daily periodic coherency, which is in accordance with the daily period found in all series in Figure 11. Moreover, all pairs except for the ones with SMF have a strong second harmonic.

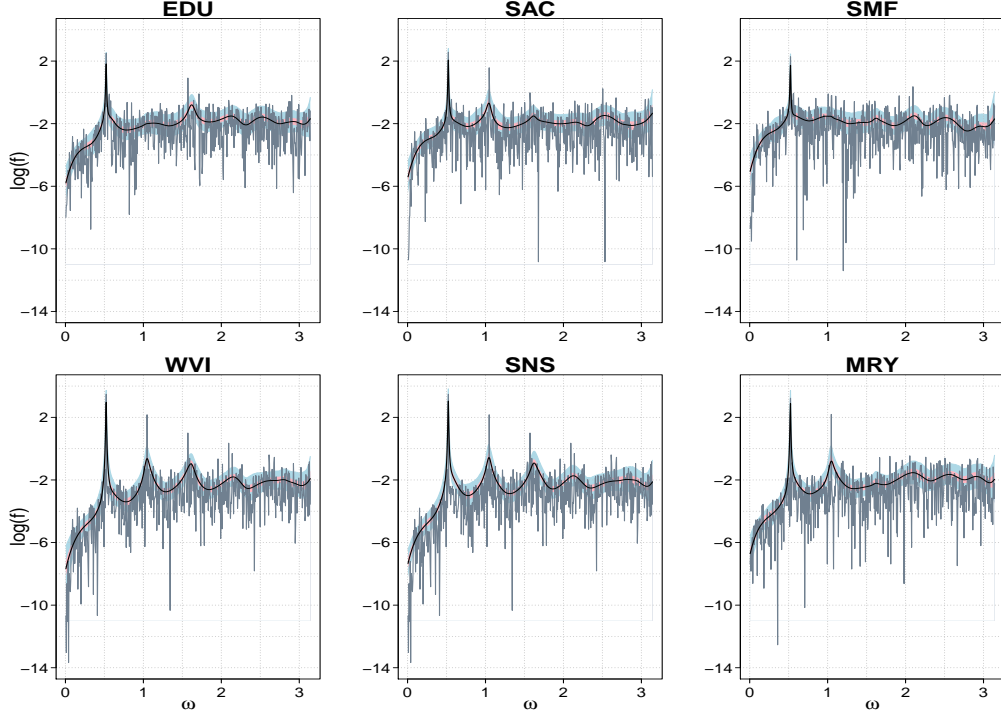


Figure 10: Logarithmic spectral estimates for the standardised detrended wind speed data by the VNPC procedure with a parametric working model with order 10. The periodogram is given by the grey line and the posterior median by the black line. The pointwise 90% posterior credible region is visualised in shaded pink and the uniform 90% region is in shaded blue.

In [Hu and Prado \(2023\)](#) correlations tend to appear locally, between locations close by, and no correlation between locations separated by 100–200 miles, i.e., between those pairs where one wind profile is taken from the group (EDU, SAC, SMF) and one from (WVI, SNS, MRY). In contrast, our results in [Figure 11](#) show high squared coherencies also between locations in different groups, most pronounced at the daily frequency. Coherencies at higher frequencies drop off more quickly for between-group pairs than within-group pairs, e.g. WVI vs. SNS as compared to WVI vs. EDU. Even over geographical distances of 100–200 miles such as between the airports in the Monterey and Sacramento region, one would expect a daily correlation between the wind profiles, however hourly or minutely patterns of the wind profiles could vary greatly between distant airports but be similar for neighbouring airports. In fact, wind speed is affected by multiple factors including wind direction,

topography and local climate. Wang et al. (2020) analysed large-scale wind patterns in California using model simulations from the variable-resolution Community Earth System Model (VR-CESM). They described ten wind patterns by directions and strengths in the northern California and patterns are associated with geopotential height pattern, geography and climate. Wind pattern is not variable with distance necessarily and wind speed correlation may not be strictly related to distance between locations.

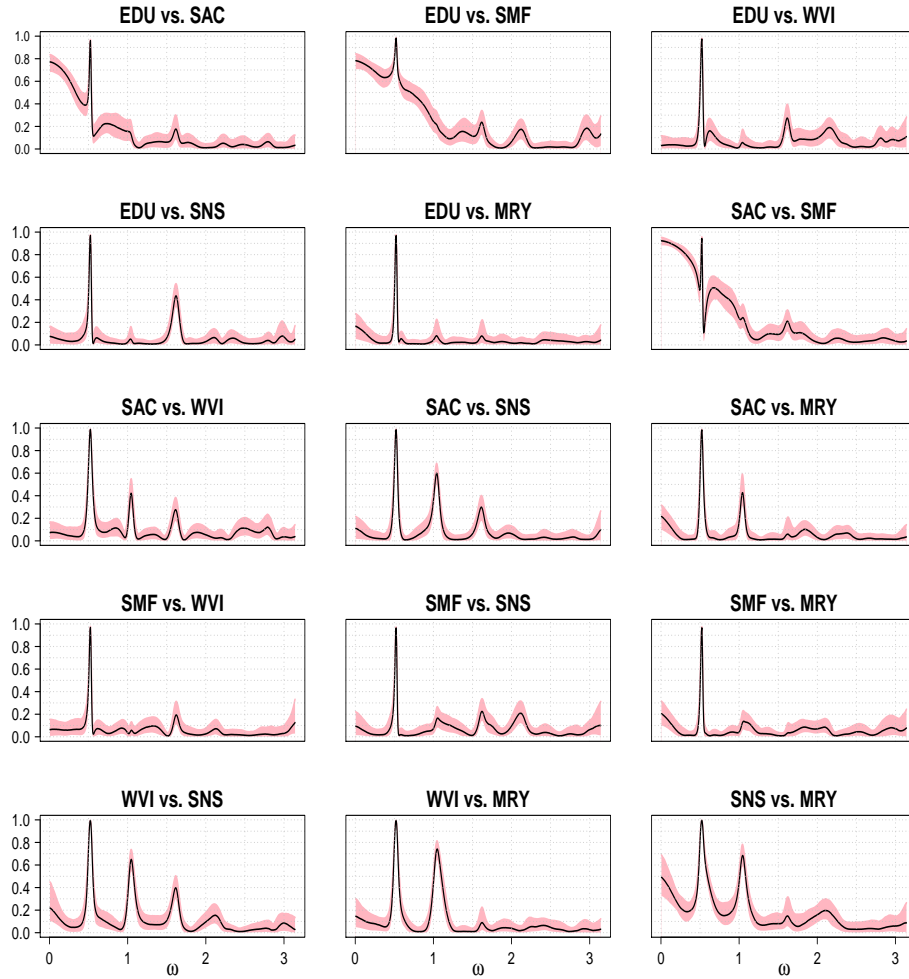


Figure 11: Estimated squared coherency for the standardised detrended wind speed data by the VNPC procedure with a parametric working model with order 10. The posterior median is given by the black line and the pointwise 90% credible region is in shaded pink.

6. Conclusion

This paper presents a novel Bayesian approach for spectral density estimation of multivariate stationary Gaussian time series. A nonparametrically corrected likelihood is proposed which can be regarded as a generalisation of the Whittle likelihood. To elaborate, a parametric likelihood is specified for the data in the time domain, and then the likelihood is nonparametrically corrected in the frequency domain in order to mitigate effects of model misspecification. A multivariate extension of the nonparametric Bernstein-Dirichlet process prior for univariate spectral densities to the space of Hermitian positive definite spectral density matrices is specified directly on the correction matrices. We prove contiguity of the nonparametrically corrected likelihood and the true likelihood for Gaussian time series. The results of a simulation study, exploring scenarios of a correctly specified parametric and a misspecified model, show that spectral density estimates based on the nonparametrically corrected likelihood inherit the efficiencies of the parametric approach in the correctly specified case and the robustness of the nonparametric approach in the misspecified case. Moreover, the nonparametrically corrected Gaussian VAR model performs well even for non-Gaussian time series. Applications demonstrate that estimates based on the nonparametrically corrected likelihood are much better in estimating sharp peaks and abrupt changes in the spectrum than nonparametric methods. R-code that implements the MCMC algorithm to sample from the posterior distribution is made publicly available at <https://github.com/easycure1/vnpctest>.

The contiguity shown in this paper is useful for deriving the posterior consistency of the corrected likelihood approach for stationary multivariate Gaussian time series based on Schwartz's theorem (Schwartz (1965)) and its extensions. The posterior consistency of our approach for the stationary multivariate non-Gaussian time series is also an exciting topic for future work. Moreover, our proposed approach holds broad applicability for analyzing multivariate stationary time series and practical utility across various datasets and disciplines, such as ECG data in medicine and gravitational waves measurements in astrophysics.

7. Supplementary section

7.1. Simulation study

In the following, we present visual representations of the spectral density estimates obtained using the three procedures for one random realisation

of the two models considered in the simulation study. These are shown in Figure S1 together the true spectral density. The individual spectra are displayed on the logarithmic scale, while real and imaginary parts of the cross spectra are on the regular scale. Figure S1 (a) shows that all three procedures have a spectral density estimate that is reasonably close to the true spectrum for the VAR(2) data. In the misspecified case, i.e., the time series generated by a VMA(1) model, the parametric VAR estimate is furthest from the true spectrum. The VNPC estimate outperforms both parametric VAR and nonparametric VNP estimate.

We consider the corresponding 90%-credible regions next, which are shown in Figure S2 for the VAR(2) realisation and Figure S3 for the VMA(1) realisation. It can be seen that the results are consistent with what we have found in Figure S1. To elaborate, for the VAR(2) example, Figure S2 shows that all three procedures yield adequate regions, while the VAR procedure with the well-specified order appears to have slightly narrower regions than the other two procedures. Figure S3 shows that the VAR estimate has much wider and more bumpy regions than the other two procedures, which demonstrates the loss of efficiency in the misspecified VMA(1) case. The VNPC and the VNP estimates have similarly narrower and smoother regions than the VAR estimate.

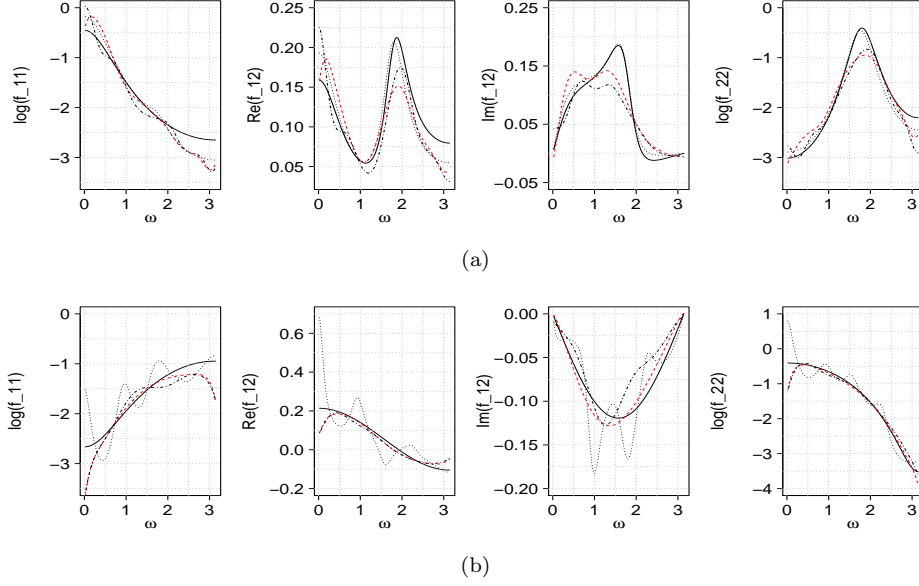


Figure S1: Spectral estimates for the realisation of (a) the VAR(2) model and (b) the VMA(1) model in Figure 1 in the article for the VNPC procedure with fixed order 1 for the parametric working model (red dashed), the VAR procedure with order selected by AIC (dotted) and the VNP procedure (dash-dotted), and the true spectral density is given by the solid black line.

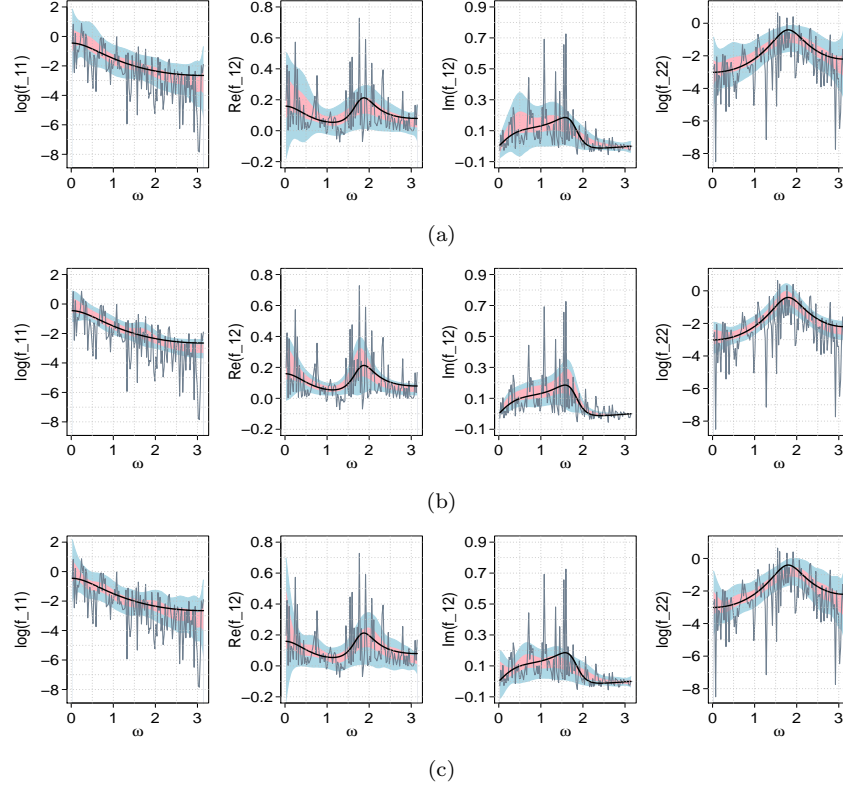


Figure S2: Posterior credible regions for the realisation of the VAR(2) model from Figure 1a in the article for (a) the VNPC procedure with fixed order 1 for the parametric working model, (b) the VAR procedure with order selected by AIC and (c) the VNP procedure. Pointwise 90% regions are represented in shaded pink, uniform 90% regions are in shaded blue, the true spectral density is given by the black solid line and the periodogram is shown in grey.

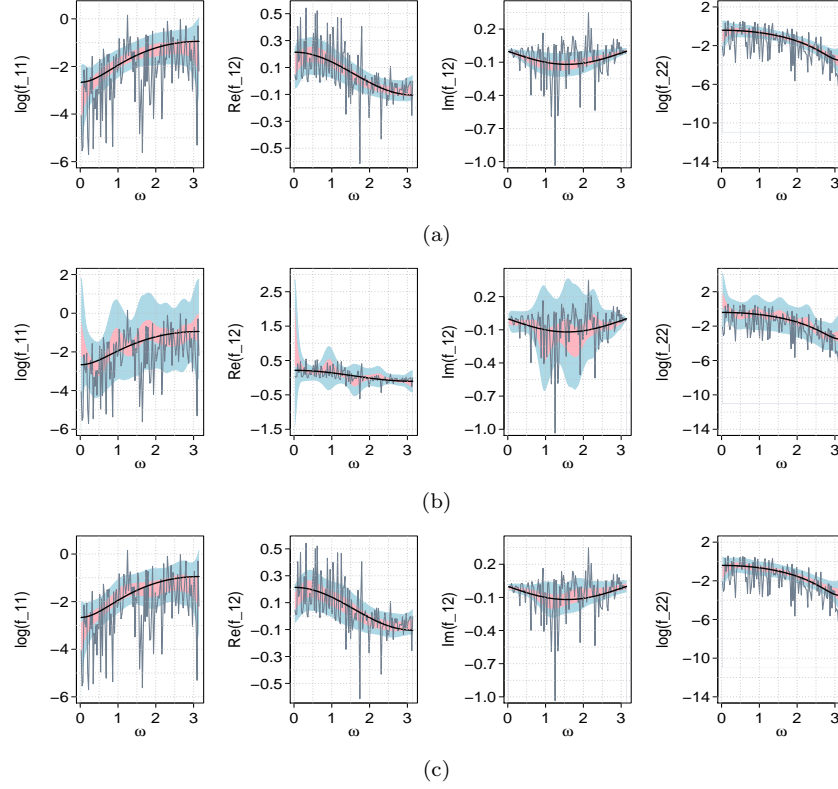


Figure S3: Posterior credible regions for the realisation of the VMA(1) model from Figure 1b in the article for (a) the VNPC procedure with fixed order 1 for the parametric working model, (b) the VAR procedure with order selected by AIC and (c) the VNP procedure. Pointwise 90% regions are visualised in shaded pink, uniform 90% regions are in shaded blue, the true spectral density is given by the black solid line and the periodogram is shown in grey.

The following simulation study considers the VAR(2) and VMA(1) models with the same coefficients and covariance matrix as (14) and (15) in the paper, while the innovation term follows a bivariate Laplace distribution rather than the Gaussian distribution. Simulation results are provided in Table S1. These clearly demonstrate that the VNPC procedure also performs well in the non-Gaussian case. Figures S4-S6 display the estimates for one $n = 256$ realisation by the three approaches.

VAR(2) model									
	$n = 256$			$n = 512$			$n = 1024$		
	VNPC(1)	VNP	VAR	VNPC(1)	VNP	VAR	VNPC(1)	VNP	VAR
L_1 -error	0.104	0.108	0.080	0.081	0.085	0.057	0.062	0.065	0.039
L_2 -error	0.135	0.138	0.105	0.107	0.111	0.074	0.082	0.087	0.051
Coverage	0.824	0.528	0.876	0.660	0.392	0.830	0.586	0.348	0.816
Width \mathbf{f}_{11}	0.339	0.315	0.202	0.177	0.171	0.120	0.110	0.105	0.076
Width $\Re \mathbf{f}_{12}$	0.253	0.229	0.144	0.169	0.159	0.087	0.118	0.113	0.055
Width $\Im \mathbf{f}_{12}$	0.209	0.183	0.120	0.139	0.126	0.074	0.096	0.089	0.049
Width \mathbf{f}_{22}	0.497	0.440	0.192	0.265	0.257	0.112	0.165	0.165	0.070
VMA(1) model									
	$n = 256$			$n = 512$			$n = 1024$		
	VNPC(1)	VNP	VAR	VNPC(1)	VNP	VAR	VNPC(1)	VNP	VAR
L_1 -error	0.094	0.109	0.163	0.069	0.080	0.125	0.054	0.059	0.096
L_2 -error	0.115	0.130	0.198	0.085	0.095	0.149	0.066	0.070	0.113
Coverage	0.870	0.574	0.958	0.798	0.450	0.954	0.648	0.314	0.948
Width \mathbf{f}_{11}	0.341	0.292	1.299	0.202	0.193	0.670	0.133	0.135	0.413
Width $\Re \mathbf{f}_{12}$	0.228	0.207	0.603	0.139	0.140	0.414	0.088	0.099	0.291
Width $\Im \mathbf{f}_{12}$	0.167	0.138	0.453	0.101	0.100	0.309	0.067	0.081	0.220
Width \mathbf{f}_{22}	0.492	0.457	1.882	0.298	0.297	0.989	0.197	0.209	0.624

Table S1: Average L_1 -, L_2 -errors, empirical coverages and median width of uniform 90% credible regions of the VNPC estimates with fixed parametric working model order 1, the VNP, and the VAR estimates with order selected by AIC for $N = 500$ realisations of the VAR(2) model (14) and the VMA(1) model (15) in the paper with a bivariate Laplace distributed innovation term.

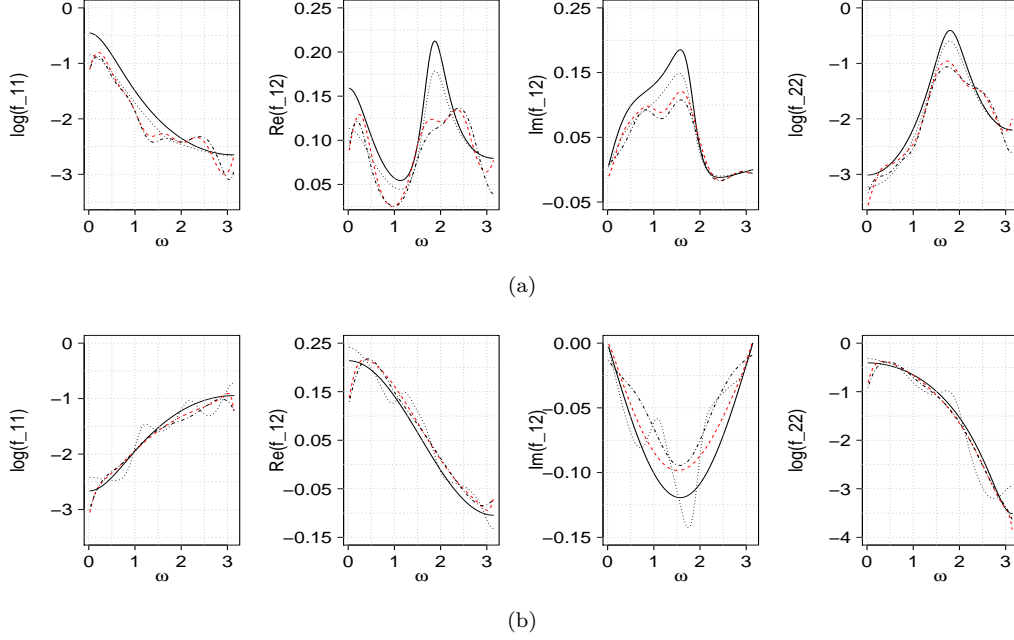


Figure S4: Spectral estimates for one realisation of (a) the VAR(2) model and (b) the VMA(1) model with a Laplace innovation of size $n = 256$ for the VNPC procedure with fixed order 1 for the parametric working model (red dashed), the VAR procedure with order selected by AIC (dotted) and the VNP procedure (dash-dotted), and the true spectral density is given by the solid black line.

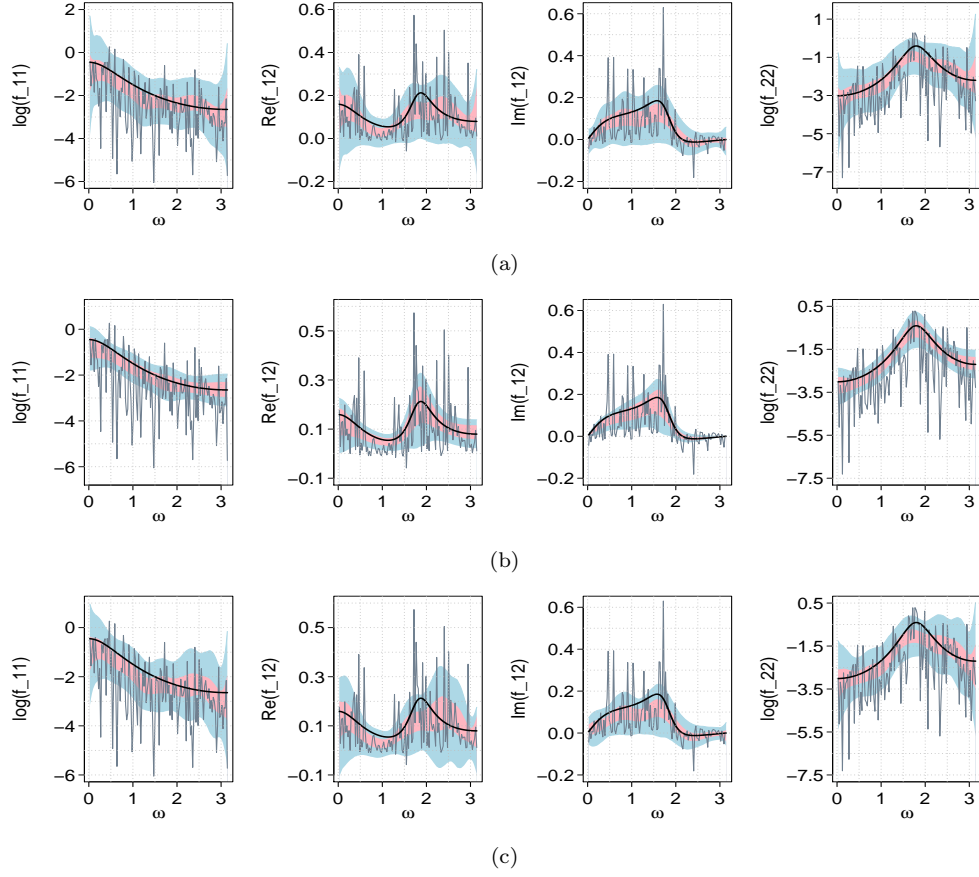


Figure S5: Posterior credible regions for the realisation of the VAR(2) model same as the one referred by Figure S4 for (a) the VNPC procedure with fixed order 1 for the parametric working model, (b) the VAR procedure with order selected by AIC and (c) the VNP procedure. Pointwise 90% regions are visualised in shaded pink, uniform 90% regions are in shaded blue, the true spectral density is given by the black solid line and the periodogram is shown in grey.

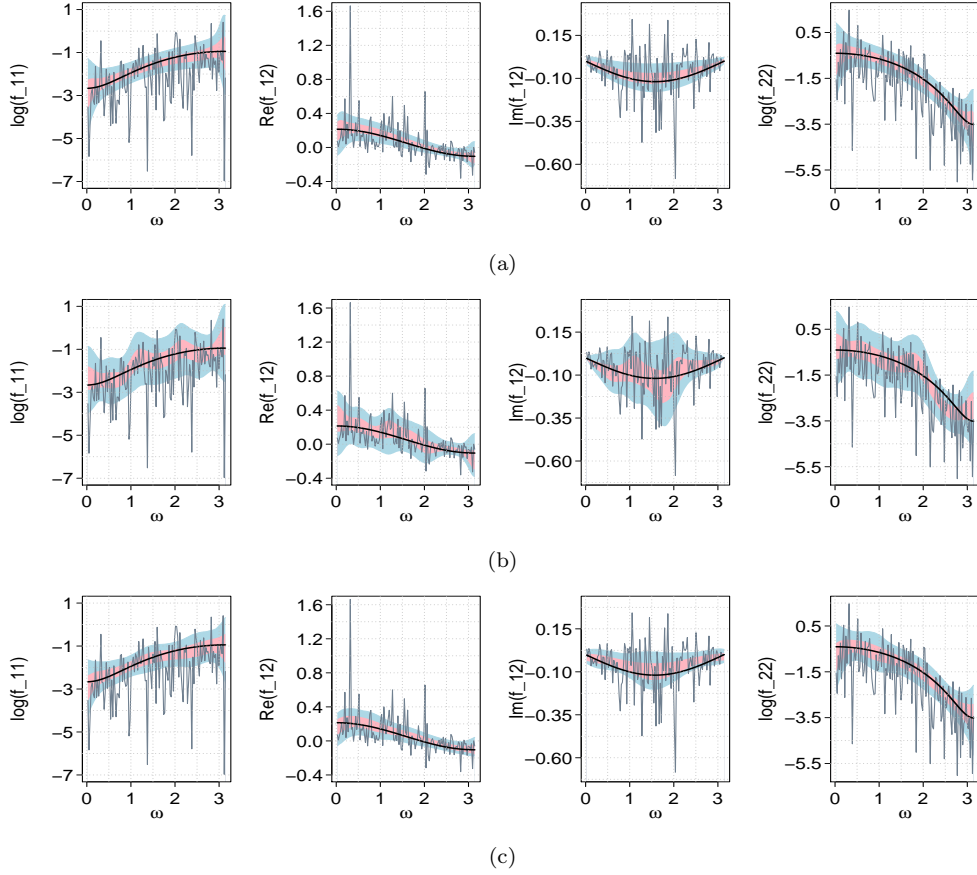


Figure S6: Posterior credible regions for the realisation of the VMA(1) model same as the one referred by Figure S4 for (a) the VNPC procedure with fixed order 1 for the parametric working model, (b) the VAR procedure with order selected by AIC and (c) the VNP procedure. Pointwise 90% regions are visualised in shaded pink, uniform 90% regions are in shaded blue, the true spectral density is given by the black solid line and the periodogram is shown in grey.

7.2. Proofs

Proof of Theorem 1. Note when $\mathbf{f} = \mathbf{f}_{\text{pa}}$, it holds that $\mathbf{C}_{nd} = \mathbf{I}_{nd}$ and $\mathbf{F}_{nd}^* \mathbf{C}_{nd}^{-1} \mathbf{F}_{nd} = \mathbf{I}_{nd}$, so (a) is proved.

To show (b), consider a time series $\underline{\mathbf{X}}_n = (\underline{X}_1, \dots, \underline{X}_n) \sim p_C^n$. Let $\underline{\mathbf{Y}}_n = \mathbf{F}_{nd}^* \mathbf{C}_{nd}^{-1} \mathbf{F}_{nd} \underline{\mathbf{X}}_n$. Because $(\mathbf{F}_{nd}^* \mathbf{C}_{nd}^{-1} \mathbf{F}_{nd})^{-1} = \mathbf{F}_{nd}^* \mathbf{C}_{nd} \mathbf{F}_{nd}$ and $|(\mathbf{F}_{nd}^* \mathbf{C}_{nd}^{-1} \mathbf{F}_{nd})^{-1}| = |\mathbf{C}_{nd}|$, we have $\underline{\mathbf{Y}}_n \sim p_{\text{pa}}$. Denote \tilde{Y}_j the Fourier coefficient of $\underline{\mathbf{Y}}_n$ at ω_j . By

Corollary 7.2.1 of [Brillinger \(2001\)](#), it follows that

$$\begin{aligned}
\mathbb{E}I_{nd,\omega_j}(\underline{\mathbf{X}}_n) &= \mathbb{E}I_{nd,\omega_j}(\mathbf{F}_{nd}^* \mathbf{C}_{nd} \mathbf{F}_{nd} \underline{\mathbf{Y}}_n) \\
&= \frac{1}{2\pi} \mathbf{C}_{nd,j} \mathbb{E} \left(\tilde{\underline{\mathbf{Y}}}_j \tilde{\underline{\mathbf{Y}}}_j^* \right) \mathbf{C}_{nd,j}^* \\
&= \mathbf{C}_{nd,j} \mathbb{E} \left(I_{nd,\omega_j}(\underline{\mathbf{Y}}_n) \right) \mathbf{C}_{nd,j}^* \\
&= \mathbf{f}^{1/2}(\omega_j) \mathbf{f}_{\text{pa}}^{-1/2}(\omega_j) \mathbf{f}_{\text{pa}}(\omega_j) \mathbf{f}_{\text{pa}}^{-1/2}(\omega_j) \mathbf{f}^{1/2}(\omega_j) + o(1) \\
&= \mathbf{f}(\omega_j) + o(1),
\end{aligned}$$

where $\mathbf{C}_{nd,j}$ is the j -th diagonal block of \mathbf{C}_{nd} .

Part (c) is shown by

$$\begin{aligned}
&\text{Cov} \left(I_{nd,\omega_j}(\underline{\mathbf{X}}_n), I_{nd,\omega_k}(\underline{\mathbf{X}}_n) \right) \\
&= \text{Cov} \left(I_{nd,\omega_j}(\mathbf{F}_{nd}^* \mathbf{C}_{nd} \mathbf{F}_{nd} \underline{\mathbf{Y}}_n), I_{nd,\omega_k}(\mathbf{F}_{nd}^* \mathbf{C}_{nd} \mathbf{F}_{nd} \underline{\mathbf{Y}}_n) \right) \\
&= \text{Cov} \left(\mathbf{C}_{nd,j} \left(\frac{1}{2\pi} \tilde{\underline{\mathbf{Y}}}_j \tilde{\underline{\mathbf{Y}}}_j^* \right) \mathbf{C}_{nd,j}^*, \mathbf{C}_{nd,k} \left(\frac{1}{2\pi} \tilde{\underline{\mathbf{Y}}}_k \tilde{\underline{\mathbf{Y}}}_k^* \right) \mathbf{C}_{nd,k}^* \right) \\
&= \text{Cov} \left(\mathbf{C}_{nd,j} I_{nd,\omega_j}(\underline{\mathbf{Y}}_n) \mathbf{C}_{nd,j}^*, \mathbf{C}_{nd,k} I_{nd,\omega_k}(\underline{\mathbf{Y}}_n) \mathbf{C}_{nd,k}^* \right).
\end{aligned}$$

□

We use a similar idea to the proof of Theorem 2.2 in [Meier et al. \(2020\)](#) to show Theorem 2. In particular, we consider a corrected likelihood for real-valued random vectors, which collect the real and imaginary parts of Fourier coefficients. Using the mapping \mathcal{B} defined in (7.7) in [Meier et al. \(2020\)](#), the real-valued version of the corrected likelihood is given by

$$p_C^n(\underline{\mathbf{Z}}_n | \mathbf{f}) \propto |\tilde{\mathbf{C}}_{nd} \tilde{\mathbf{C}}_{nd}^T|^{-1/2} p_{\text{pa}}^n(\tilde{\mathbf{F}}_{nd}^T \tilde{\mathbf{C}}_{nd}^{-1} \tilde{\mathbf{F}}_{nd} \underline{\mathbf{Z}}_n), \quad (17)$$

with

$$\tilde{\mathbf{C}}_{nd} := \begin{pmatrix} \mathbf{f}^{1/2}(0) \mathbf{f}_{\text{pa}}^{-1/2}(0) & & & \\ & \mathcal{B}(\mathbf{f}^{1/2}(\omega_1) \mathbf{f}_{\text{pa}}^{-1/2}(\omega_1)) & & \\ & & \ddots & \\ & & & \mathcal{B}(\mathbf{f}^{1/2}(\omega_N) \mathbf{f}_{\text{pa}}^{1/2}(\omega_N)) \\ & & & & \mathbf{f}^{1/2}(\pi) \mathbf{f}_{\text{pa}}^{-1/2}(\pi) \end{pmatrix}$$

for n even and

$$\tilde{\mathbf{C}}_{nd} := \begin{pmatrix} \mathbf{f}^{1/2}(0)\mathbf{f}_{\text{pa}}^{-1/2}(0) & & & \\ & \mathcal{B}(\mathbf{f}^{1/2}(\omega_1)\mathbf{f}_{\text{pa}}^{-1/2}(\omega_1)) & & \\ & & \ddots & \\ & & & \mathcal{B}(\mathbf{f}^{1/2}(\omega_N)\mathbf{f}_{\text{pa}}^{1/2}(\omega_N)) \end{pmatrix}$$

for n odd, where $\tilde{\mathbf{F}}_{nd}$ is a real-valued multivariate discrete Fourier transform operator and orthogonal.

Proof of Theorem 2. Meier et al. (2020) have proved the mutual contiguity of the full Gaussian likelihood and the Whittle likelihood (see Theorem 2.2 in the article). Therefore, we only need to show the mutual contiguity of the joint densities under the Whittle likelihood and the corrected likelihood. To this end, we use the real-valued corrected likelihood (17) and follow the arguments from the proof of the mutual contiguity of the Whittle likelihood and the true Gaussian likelihood in the univariate case in Choudhuri et al. (2004b). Then, it is sufficient to show the tightness of

$$\begin{aligned} \log \frac{P_C^n}{P_W^n} &\propto -\frac{1}{2} \left(\log |\tilde{\mathbf{C}}_{nd}\tilde{\mathbf{C}}_{nd}^T| + \log |\mathbf{\Gamma}_{nd,\text{pa}}| - \log |\tilde{\mathbf{D}}_{nd}| \right) \\ &\quad - \frac{1}{2} \left(\underline{\mathbf{Z}}_n^T \tilde{\mathbf{F}}_{nd}^T \tilde{\mathbf{C}}_{nd}^{-1T} \tilde{\mathbf{F}}_{nd} \mathbf{\Gamma}_{nd,\text{pa}}^{-1} \tilde{\mathbf{F}}_{nd}^T \tilde{\mathbf{C}}_{nd}^{-1} \tilde{\mathbf{F}}_{nd} \underline{\mathbf{Z}}_n - \underline{\mathbf{Z}}_n^T \tilde{\mathbf{F}}_{nd}^T \tilde{\mathbf{D}}_{nd}^{-1} \tilde{\mathbf{F}}_{nd} \underline{\mathbf{Z}}_n \right) \\ &:= -\frac{1}{2} \mathbf{A}_n - \frac{1}{2} \mathbf{B}_n, \end{aligned} \tag{18}$$

where

$$P_W^n \propto |\tilde{\mathbf{D}}_{nd}|^{-1/2} \exp \left\{ -\frac{1}{2} \underline{\mathbf{Z}}_n^T \tilde{\mathbf{F}}_{nd}^T \tilde{\mathbf{D}}_{nd}^{-1} \tilde{\mathbf{F}}_{nd} \underline{\mathbf{Z}}_n \right\}$$

with $\tilde{\mathbf{D}}_{nd}$ defined in (7.7) in Meier et al. (2020) and

$$P_C^n \propto |\tilde{\mathbf{C}}_{nd}\tilde{\mathbf{C}}_{nd}^T|^{-1/2} |\mathbf{\Gamma}_{nd,\text{pa}}|^{-1/2} \exp \left\{ -\frac{1}{2} \underline{\mathbf{Z}}_n^T \tilde{\mathbf{F}}_{nd}^T \tilde{\mathbf{C}}_{nd}^{-1T} \tilde{\mathbf{F}}_{nd} \mathbf{\Gamma}_{nd,\text{pa}}^{-1} \tilde{\mathbf{F}}_{nd}^T \tilde{\mathbf{C}}_{nd}^{-1} \tilde{\mathbf{F}}_{nd} \underline{\mathbf{Z}}_n \right\}.$$

Let $\tilde{\mathbf{D}}_{nd,\text{pa}} := \tilde{\mathbf{C}}_{nd}^{-1} \tilde{\mathbf{D}}_{nd} \tilde{\mathbf{C}}_{nd}^{-T}$. Clearly, it follows that

$$\log |\tilde{\mathbf{D}}_{nd}| - \log |\tilde{\mathbf{C}}_{nd}\tilde{\mathbf{C}}_{nd}^T| = \log |\tilde{\mathbf{C}}_{nd}^{-1} \tilde{\mathbf{D}}_{nd} \tilde{\mathbf{C}}_{nd}^{-T}| = \log |\tilde{\mathbf{D}}_{nd,\text{pa}}|.$$

In terms of Lemma 7.1 and the same arguments in Meier et al. (2020), it holds $\mathbf{A}_n = \log |\mathbf{\Gamma}_{nd,\text{pa}}| - \log |\tilde{\mathbf{D}}_{nd,\text{pa}}| = O(1)$ as $n \rightarrow \infty$.

Let $\tilde{\mathbf{\Gamma}}_{nd,pa} := \tilde{\mathbf{F}}_{nd} \mathbf{\Gamma}_{nd,pa} \tilde{\mathbf{F}}_{nd}^T$, then $\tilde{\mathbf{\Gamma}}_{nd,pa}^{-1} = \tilde{\mathbf{F}}_{nd} \mathbf{\Gamma}_{nd,pa}^{-1} \tilde{\mathbf{F}}_{nd}^T$. Under P_C^n , it follows $\tilde{\mathbf{Z}}_n := \tilde{\mathbf{F}}_{nd} \mathbf{Z}_n \sim N(\mathbf{0}, \tilde{\mathbf{C}}_{nd} \tilde{\mathbf{F}}_{nd} \mathbf{\Gamma}_{nd,pa} \tilde{\mathbf{F}}_{nd}^T \tilde{\mathbf{C}}_{nd}^T)$. Following the arguments of the proofs in Choudhuri et al. (2004b) and Meier et al. (2020), it holds that

$$\begin{aligned} \mathbb{E}_{P_C^n} \mathbf{B}_n &= \text{tr} \left[\left(\tilde{\mathbf{C}}_{nd}^{-T} \tilde{\mathbf{F}}_{nd} \mathbf{\Gamma}_{nd,pa}^{-1} \tilde{\mathbf{F}}_{nd}^T \tilde{\mathbf{C}}_{nd}^{-1} - \tilde{\mathbf{D}}_{nd}^{-1} \right) \tilde{\mathbf{C}}_{nd} \tilde{\mathbf{F}}_{nd} \mathbf{\Gamma}_{nd,pa} \tilde{\mathbf{F}}_{nd}^T \tilde{\mathbf{C}}_{nd}^T \right] \\ &= \text{tr} \left(\mathbf{I}_{nd} - \tilde{\mathbf{\Gamma}}_{nd,pa} \tilde{\mathbf{D}}_{nd,pa}^{-1} \right) \end{aligned}$$

and

$$\begin{aligned} \text{Var}_{P_C^n} \mathbf{B}_n &= 2 \text{tr} \left[\left(\tilde{\mathbf{C}}_{nd} \tilde{\mathbf{F}}_{nd} \mathbf{\Gamma}_{nd,pa} \tilde{\mathbf{F}}_{nd}^T \tilde{\mathbf{C}}_{nd}^T \left(\tilde{\mathbf{C}}_{nd}^{-T} \tilde{\mathbf{F}}_{nd} \mathbf{\Gamma}_{nd,pa}^{-1} \tilde{\mathbf{F}}_{nd}^T \tilde{\mathbf{C}}_{nd}^{-1} - \tilde{\mathbf{D}}_{nd}^{-1} \right) \right)^2 \right] \\ &= 2 \text{tr} \left[\left(\mathbf{I}_{nd} - \tilde{\mathbf{\Gamma}}_{nd,pa} \tilde{\mathbf{D}}_{nd,pa}^{-1} \right)^2 \right]. \end{aligned}$$

Let $\mathbf{H}_{nd,pa} := \tilde{\mathbf{\Gamma}}_{nd,pa} - \tilde{\mathbf{D}}_{nd,pa} \in \mathbb{R}^{nd \times nd}$. By Lemma 7.3 in Meier et al. (2020) and $|\text{tr}(\mathbf{A}\mathbf{B})| \leq \|\mathbf{A}\| \|\mathbf{B}\|$ for any $\mathbf{A}, \mathbf{B} \in \mathbb{R}^{d \times d}$ and the Frobenius norm $\|\cdot\|$, it yields that

$$\left| \mathbb{E}_{P_C^n} \mathbf{B}_n \right| \lesssim \left(\left\lfloor \frac{n}{2} \right\rfloor + 1 \right) n^{-1} b_{0,pa}^{-1} = O(1)$$

with $b_{0,pa}$ from Assumption 1, where $a_n \lesssim b_n$ indicates that there exists a positive constant C such that $a_n \leq C b_n$ for all n . It also can be shown that

$$\text{Var}_{P_C^n} \mathbf{B}_n \lesssim \left(\left\lfloor \frac{n}{2} \right\rfloor + 1 \right)^2 n^{-2} b_{0,pa}^{-2} = O(1).$$

Under P_W^n , it holds $\tilde{\mathbf{Z}}_n = \tilde{\mathbf{F}}_{nd} \mathbf{Z}_n \sim N(\mathbf{0}, \tilde{\mathbf{D}}_{nd})$. Similarly, we have

$$\begin{aligned} \mathbb{E}_{P_W^n} \mathbf{B}_n &= \text{tr} \left[\left(\tilde{\mathbf{C}}_{nd}^{-T} \tilde{\mathbf{F}}_{nd} \mathbf{\Gamma}_{nd,pa}^{-1} \tilde{\mathbf{F}}_{nd}^T \tilde{\mathbf{C}}_{nd}^{-1} - \tilde{\mathbf{D}}_{nd}^{-1} \right) \tilde{\mathbf{D}}_{nd} \right] \\ &= \text{tr} \left(\tilde{\mathbf{D}}_{nd,pa} \tilde{\mathbf{\Gamma}}_{nd,pa}^{-1} - \mathbf{I}_{nd} \right) \end{aligned}$$

and

$$\begin{aligned} \text{Var}_{P_W^n} \mathbf{B}_n &= 2 \text{tr} \left[\left(\tilde{\mathbf{D}}_{nd} \left(\tilde{\mathbf{C}}_{nd}^{-T} \tilde{\mathbf{F}}_{nd} \mathbf{\Gamma}_{nd,pa}^{-1} \tilde{\mathbf{F}}_{nd}^T \tilde{\mathbf{C}}_{nd}^{-1} - \tilde{\mathbf{D}}_{nd}^{-1} \right) \right)^2 \right] \\ &= 2 \text{tr} \left[\left(\tilde{\mathbf{D}}_{nd,pa} \tilde{\mathbf{\Gamma}}_{nd,pa}^{-1} - \mathbf{I}_{nd} \right)^2 \right]. \end{aligned}$$

By the same arguments of the proof of Theorem 2.2 in Meier et al. (2020), it holds $|\mathbb{E}_{P_W^n} \mathbf{B}_n| = O(1)$ and $\text{Var}_{P_W^n} \mathbf{B}_n = O(1)$. Then, the proof is concluded. \square

References

- Aicher, C., Ma, Y.A., Foti, N.J., Fox, E.B., 2019. Stochastic gradient MCMC for state space models. *SIAM J. Math. Anal.* 1(3), 555–587. DOI: [10.1137/18M1214780](https://doi.org/10.1137/18M1214780).
- Akaike, H., 1974. A new look at the statistical model identification. *IEEE Trans. Automat. Contr.* 19, 716–723. DOI: [10.1109/TAC.1974.1100705](https://doi.org/10.1109/TAC.1974.1100705).
- Barigozzi, M., Hallin, M., 2016. Generalized dynamic factor models and volatilities: recovering the market volatility shocks. *Econom. J.* 19(1), C33–C60. DOI: [10.1111/ectj.12047](https://doi.org/10.1111/ectj.12047).
- Berkowitz, J., Diebold, F.X., 1998. Bootstrapping multivariate spectra. *Rev. Econ. Stat.* 80(4), 664–666. DOI: [10.1162/003465398557753](https://doi.org/10.1162/003465398557753).
- Brillinger, D.R., 2001. *Time Series: Data Analysis and Theory. Classics in Applied Mathematics*, Society for Industrial and Applied Mathematics, Philadelphia.
- Brockwell, P.J., Davis, R.A., 1991. *Time series: Theory and methods*. 2nd ed., Springer, New York.
- Cadonna, A., Kottas, A., Prado, R., 2017. Bayesian mixture modeling for spectral density estimation. *Stat. Probab. Lett.* 125, 189–195. DOI: [10.1016/j.spl.2017.02.008](https://doi.org/10.1016/j.spl.2017.02.008).
- Cadonna, A., Kottas, A., Prado, R., 2019. Bayesian spectral modeling for multiple time series. *J. Am. Stat. Assoc.* 114(528), 1838–1853. DOI: [10.1080/01621459.2018.1520114](https://doi.org/10.1080/01621459.2018.1520114).
- Carvalho, C.M., Chang, J., Lucas, J.E., Nevins, J.R., Wang, Q., West, M., 2008. High-dimensional sparse factor modeling: applications in gene expression genomics. *J. Am. Stat. Assoc.* 103(484), 1438–1456. DOI: [10.1198/016214508000000869](https://doi.org/10.1198/016214508000000869).
- Choudhuri, N., Ghosal, S., Roy, A., 2004a. Bayesian estimation of the spectral density of a time series. *J. Am. Stat. Assoc.* 99, 1050–1059. DOI: [10.1198/016214504000000557](https://doi.org/10.1198/016214504000000557).

- Choudhuri, N., Ghosal, S., Roy, A., 2004b. Contiguity of the Whittle measure for a Gaussian time series. *Biometrika* 91, 211–218. DOI: [10.1214/18-BA1126](https://doi.org/10.1214/18-BA1126).
- Dai, M., Guo, W., 2004. Multivariate spectral analysis using Cholesky decomposition. *Biometrika* 91(3), 629–643. DOI: [10.1093/biomet/91.3.629](https://doi.org/10.1093/biomet/91.3.629).
- Edwards, M.C., Meyer, R., Christensen, N., 2019. Bayesian nonparametric spectral density estimation using B-spline priors. *Stat. Comput.* 29(1), 67–78. DOI: [10.1007/s11222-017-9796-9](https://doi.org/10.1007/s11222-017-9796-9).
- Fiecas, M., 2014. Data-driven shrinkage of the spectral density matrix of a high-dimensional time series. *Electron. J. Stat.* 8(2), 2975–3003. DOI: [10.1214/14-EJS977](https://doi.org/10.1214/14-EJS977).
- Fox, E.B., Hughes, M.C., Sudderth, E.B., Jordan, M.I., 2014. Joint modeling of multiple times series via the beta process with application to motion capture segmentation. *Ann. Appl. Stat.* 8(3), 1281–1313. DOI: [10.1214/14-AOAS742](https://doi.org/10.1214/14-AOAS742).
- Fox, E.B., Sudderth, E.B., Jordan, M.I., Willsky, A.S., 2011. Bayesian non-parametric inference of switching dynamic linear models. *IEEE Trans. Signal Process.* 59(4), 1569–1585. DOI: [10.1109/TSP.2010.2102756](https://doi.org/10.1109/TSP.2010.2102756).
- Franke, J., Hardle, W., 1992. On bootstrapping kernel spectral estimates. *Ann. Stat.* 20(1), 121–145. DOI: [10.1214/aos/1176348515](https://doi.org/10.1214/aos/1176348515).
- Hastings, W.K., 1970. Monte Carli sampling methods using Markov chains and their applications. *Biometrika* 57(1), 97–109. DOI: [10.1093/biomet/57.1.97](https://doi.org/10.1093/biomet/57.1.97).
- Hu, Z., Prado, R., 2023. Fast Bayesian inference on spectral analysis of multivariate stationary time series. *Comput. Stat. Data Anal.* 178, 107596. DOI: [10.1016/j.csda.2022.107596](https://doi.org/10.1016/j.csda.2022.107596).
- Iowa State University, 2022. Iowa environmental mesonet. <https://mesonet.agron.iastate.edu/>. Accessed: 2022-12-19.
- Jentsch, C., Kreiss, J.P., 2010. The multiple hybrid bootstrap - resampling multivariate linear processes. *J. Multivar. Anal.* 101(10), 2320–2345. DOI: [10.1016/j.jmva.2010.06.005](https://doi.org/10.1016/j.jmva.2010.06.005).

- Jentsch, C., Politis, D.N., 2015. Covariance matrix estimation and linear process bootstrap for multivariate time series of possible increasing dimension. *Ann. Stat.* 43(3), 1117–1140. DOI: [10.1214/14-AOS1301](https://doi.org/10.1214/14-AOS1301).
- Kalli, M., Griffin, J.E., 2018. Bayesian nonparametric vector autoregressive models. *J. Econom.* 203(2), 267–282. DOI: [10.1016/j.jeconom.2017.11.009](https://doi.org/10.1016/j.jeconom.2017.11.009).
- Kastner, G., Huber, F., 2020. Sparse Bayesian vector autoregressions in huge dimensions. *J. Forecast.* 39(7), 1142–1165. DOI: [10.1002/for.2680](https://doi.org/10.1002/for.2680).
- Kirch, C., Edwards, M.C., Meier, A., Meyer, R., 2019. Beyond Whittle: nonparametric correction of a parametric likelihood with a focus on Bayesian time series analysis. *Bayesian Anal.* 14, 1037–1073. DOI: [10.1214/18-BA1126](https://doi.org/10.1214/18-BA1126).
- Kirch, C., Politis, D.N., 2011. TFT-bootstrap: resampling time series in the frequency domain to obtain replicates in the time domain. *Ann. Stat.* 39(3), 1427–1470. DOI: [10.1214/10-AOS868](https://doi.org/10.1214/10-AOS868).
- Koop, G., Korobilis, D., 2010. Bayesian multivariate time series methods for empirical macroeconomics. *Found. Trends Econom.* 3, 267–358.
- Krafty, R.T., Collinge, W.O., 2013. Penalized multivariate Whittle likelihood for power spectrum estimation. *Biometrika* 100(2), 447–458. DOI: [10.1093/biomet/ass088](https://doi.org/10.1093/biomet/ass088).
- Krampe, J., Kreiss, J.P., Paparoditis, E., 2019. Bootstrap based inference for sparse high-dimensional time series models. *arXiv preprint ArXiv:1806.11083v3*.
- Kreiss, J.P., Paparoditis, E., 2003. Autoregressive-aided periodogram bootstrap for time series. *Ann. Stat.* 31(6), 1923–1955. DOI: [10.1214/aos/1074290332](https://doi.org/10.1214/aos/1074290332).
- Lütkepohl, H., 2005. *New Introduction to Multiple Time Series Analysis*. Springer Berlin, Heidelberg.
- Mannarano, D., 1998. Automated surface observing system (ASOS) users’s guide. <https://www.weather.gov/media/asos/aum-toc.pdf>.

- Maturana-Russel, P., Meyer, R., 2021. Bayesian spectral density estimation using P-splines with quantile-based knot placement. *Comput. Stat.* 36(3), 2055–2077. DOI: [10.1007/s00180-021-01066-7](https://doi.org/10.1007/s00180-021-01066-7).
- McMurry, T.L., Politis, D.N., 2010. Banded and tapered estimates for auto-covariance matrices and the linear process bootstrap. *J. Time Ser. Anal.* 31(6), 471–482. DOI: [10.1111/j.1467-9892.2010.00679.x](https://doi.org/10.1111/j.1467-9892.2010.00679.x).
- Meier, A., 2018. A matrix Gamma process and applications to Bayesian analysis of multivariate time series. Ph.D. thesis. Otto von Guericke University Magdeburg. DOI: [10.25673/13407](https://doi.org/10.25673/13407).
- Meier, A., Kirch, C., Edwards, M.C., Meyer, R., 2022. beyondWhittle: Bayesian Spectral Inference for Stationary Time Series. R package version 1.1.3. <https://cran.r-project.org/web/packages/beyondWhittle/>.
- Meier, A., Kirch, C., Meyer, R., 2020. Bayesian nonparametric analysis of multivariate time series: a matrix Gamma process approach. *J. Multivar. Anal.* 175. DOI: [10.1016/j.jmva.2019.104560](https://doi.org/10.1016/j.jmva.2019.104560).
- Meyer, M., Kreiss, J., 2015. On the vector autoregressive sieve bootstrap. *J. Time. Ser. Anal.* 36(3), 377–397. DOI: [10.1111/jtsa.12090](https://doi.org/10.1111/jtsa.12090).
- Muliere, P., Tardella, T., 1998. Approximating distributions of random functionals of Ferguson-Dirichlet priors. *Can. J. Stat.* 26, 283–297. DOI: [10.2307/3315511](https://doi.org/10.2307/3315511).
- National Oceanic and Atmospheric Administration, 2022. El Niño/southern oscillation (ENSO). <https://www.ncei.noaa.gov/access/monitoring/enso>. Accessed: 2022-11-13.
- Rao, S.S., Yang, J., 2021. Reconciling the Gaussian and Whittle likelihood with an application to estimation in the frequency domain. *Ann. Stat.* 49(5), 2774–2802. DOI: [10.1214/21-AOS2055](https://doi.org/10.1214/21-AOS2055).
- Rodríguez, A., Dunson, D.B., 2011. Nonparametric Bayesian models through probit stick-breaking processes. *Bayesian Anal.* 6(1), 145–178. DOI: [10.1214/11-BA605](https://doi.org/10.1214/11-BA605).
- Rosen, O., Stoffer, D.S., 2007. Automatic estimation of multivariate spectra via smoothing splines. *Biometrika* 94(2), 335–345. DOI: [10.1093/biomet/asm022](https://doi.org/10.1093/biomet/asm022).

- Rousseau, J., Chopin, N., Liso, B., 2012. Bayesian nonparametric estimation of the spectral density of a long or intermediate memory Gaussian process. *Ann. Stat.* 40(2), 964–995. DOI: [10.1214/11-AOS955](https://doi.org/10.1214/11-AOS955).
- Schwartz, L., 1965. On Bayes procedures. *Z. Wahrsch. Verw. Gebiete* 4, 10–26.
- Shao, X., Wu, W.B., 2007. Asymptotic spectral theory for nonlinear time series. *The Annals of statistics* 35, 1773–1801.
- Shumway, R.H., Stoffer, D.S., 2011. *Time Series Analysis and Its Applications With R Examples*. 3rd ed., Springer, New York.
- Statistics New Zealand, 2020. El Niño southern oscillation. <https://www.stats.govt.nz/indicators/el-nino-southern-oscillation>. Accessed: 2022-11-13.
- Stoffer, D., 2022. *astsa: Applied Statistical Time Series Analysis*. R package version 1.16. <https://cran.r-project.org/web/packages/astsa/>.
- Szabó, B., van der Vaart, A.W., van Zanten, J.H., 2015. Frequentist coverage of adaptive nonparametric Bayesian credible sets. *Ann. Statist.* 43(4), 1391–1428. DOI: [10.1214/14-AOS1270](https://doi.org/10.1214/14-AOS1270).
- Tierney, L., 1994. Markov chains for exploring posterior distributions. *Ann. Stat.* 22(4), 1701–1762. DOI: [10.1214/aos/1176325750](https://doi.org/10.1214/aos/1176325750).
- van der Vaart, A.W., 1998. *Asymptotic statistics*. volume 3. Cambridge University Press, Cambridge, UK.
- Wang, M., Ullrich, P., Millstein, D., 2020. Future projections of wind patterns in california with the variable-resolution cesm: a clustering analysis approach. *Clim. Dyn.* 54, 2511–2531. DOI: [10.1007/s00382-020-05125-5](https://doi.org/10.1007/s00382-020-05125-5).
- Whittle, P., 1957. Curve and periodogram smoothing. *J. R. Stat. Soc. Series B Stat. Methodol.* 19(1), 38–63. DOI: [10.1111/j.2517-6161.1957.tb00242.x](https://doi.org/10.1111/j.2517-6161.1957.tb00242.x).